# Tectonic and climatic controls on knickpoint retreat rates and landscape response times

Alexander C. Whittaker[1] and Sarah J. Boulton[2]

[1]   The rate at which transient knickpoints propagate through a landscape fundamentally controls the rate of geomorphic response to tectonic and climatic perturbation. Here we present knickpoint retreat rates upstream of active faults for 19 bedrock catchments in Turkey and 11 bedrock catchments in Italy where we have very good constraints on both the magnitude and timing of the tectonic perturbation and where climate histories are well documented. We show that the knickpoints have average retreat rates of between 0.2 and 2 mm/yr for catchments with drainage areas between 6 and 65 km$^2$ and we test whether differences in rock mass strength and catchment size are sufficient to explain this range in retreat rates. Our analysis suggests that even accounting for these two variables, knickpoint propagation velocities differ markedly, and we show that channels crossing faults with higher throw rates have knickpoints that are retreating faster. The dependence of knickpoint retreat velocity on throw rate is at least as important as catchment drainage area. These results indicate, counterintuitively, that landscapes forced by large amplitude tectonic perturbations will have shorter response times than those perturbed by smaller amplitude changes. The link between the knickpoint propagation velocity and throw rate is largely (but not completely) explained by channel narrowing in areas of high uplift rate. Channel steepening upstream of the active faults may explain all of the residual dependency of knickpoint retreat rate on fault throw rate, but only if the slope exponent, $n$, in the standard stream power model is greater than 1.3. However, we cannot rule out a role for sediment supply in driving enhanced knickpoint retreat rate in addition to the well-documented channel narrowing effect. Finally, we find that mean knickpoints retreat rates in Turkey are only half of those in Italy, for catchments of equivalent size, crossing faults with similar throw rates. This difference in fluvial response time is accounted for by long-term differences in the ratio of precipitation to infiltration in the two areas over the last 1 My.

## 1. Introduction

[2]   Constraining landscape response times to tectonic or climatic perturbation remains a key challenge within the geosciences [*Whittaker et al.*, 2007a; *Reinhardt et al.*, 2007; *Allen*, 2008; *Tucker*, 2009], particularly because knowledge of geomorphic response times is vital in order to predict landscape sensitivity to future environmental change. To address this challenge effectively it is necessary to understand and quantify the transient dynamics of upland river systems to external perturbation, as the fluvial network determines the relief structure of mountain belts [*Whipple and Tucker*, 1999; *Reinhardt et al.*, 2007; *Mudd and Furbish*, 2007; *Brocklehurst*, 2010] and physically transmits tectonic and climatic signals to the landscape [e.g., *Tucker*, 2009; *Brocklehurst*, 2010, for recent reviews]. Workers have made considerable progress in developing and discriminating between competing sets of fluvial erosion "laws" [*Howard et al.*, 1994; *Tucker and Whipple*, 2002; *Whipple and Tucker*, 2002; *Sklar and Dietrich*, 2004], developing improved models of landscape evolution [*Tucker et al.*, 2001; *Attal et al.*, 2008; *Tucker*, 2009]; using DEM and field-based methodologies to evaluate the extent to which fluvially sculpted landscapes embed tectono-climatic signals in channel long profiles; in metrics based on slope-area plots [e.g., *Kirby et al.*, 2003; *Wobus et al.*, 2006a; *DiBiase et al.*, 2010]; and in aspects of their channel geometry [*Whittaker et al.*, 2008; *Boulton and Whittaker*, 2009].

[1]Department of Earth Science and Engineering, Royal School of Mines, Imperial College, London, UK.
[2]School of Geography, Earth and Environmental Sciences, University of Plymouth, Plymouth, Devon, UK.

Corresponding author: A. C. Whittaker, Department of Earth Science and Engineering, Royal School of Mines, Imperial College, South Kensington Campus, London, SW7 2AZ, UK. (a.whittaker@imperial.ac.uk)

[3] Central to understanding landscape response times within the above framework are improved constraints on the evolution and migration of "knickpoints" or "knickzones" in fluvial systems [*Bishop et al.*, 2005; *Crosby and Whipple*, 2006; *Berlin and Anderson*, 2007; *Attal et al.*, 2011]. While the term "knickpoint" is sometimes used to describe discrete features such as waterfalls, in this paper we use the term "knickzone" to mean a steep reach of a channel which creates a local convexity in what would otherwise be a concave-up long profile of a river and "knickpoint" to indicate the precise point in the long profile where the rate of change of channel gradient is a maximum [cf. *Crosby and Whipple*, 2006; *Whittaker et al.*, 2008]. Knickpoints can be formed and pinned at lithological boundaries where rock strength differs [e.g., *Stock and Montgomery*, 1999]; however, we focus on knickpoint formation and migration in response to external perturbation that results in enhanced bedrock incision, such as a relative increase in tectonic uplift rate, or a base level fall at a catchment outlet. Theoretical, observational and modeling studies have all shown that when bedrock channels (i.e., those close to the detachment-limited erosional end-member [sensu *Tucker and Whipple*, 2002]) are perturbed from topographic steady state by these mechanisms, a steep transient knickzone develops as the channel adjusts its form to incise and keep pace with the new boundary conditions [*Tucker and Whipple*, 2002; *Crosby and Whipple*, 2006; *Whittaker et al.*, 2007a]. The knickpoint separates an incised downstream part of the catchment that has adjusted to a perturbation, such as an increased slip rate on a fault, from the rest of the catchment that is yet to respond to the boundary condition change [*Whittaker et al.*, 2007b; *Berlin and Anderson*, 2007]. Knickpoints are commonly observed or inferred to have retreated upstream over time [e.g., *Weissel and Seidl*, 1998; *Bishop et al.*, 2005; *Berlin and Anderson*, 2007; *Attal et al.*, 2008; *Whittaker et al.*, 2008; *Jansen et al.*, 2011], although opinions differ as to the dominant physical mechanism by which this occurs [e.g., *Berlin and Anderson*, 2009]. Upstream migration of a knickpoint gives rise to a wave of incision that progressively transmits the signal of boundary condition change to the whole catchment area [*Tucker and Whipple*, 2002; *Harkins et al.*, 2007; *Whittaker et al.*, 2010]. A number of studies have addressed transient landscape evolution from this perspective, while also incorporating new constraints on the evolution of channel geometry [e.g., *Tucker and Whipple*, 2002; *Whittaker et al.*, 2007b; *Attal et al.*, 2008]. For example *Whittaker et al.* [2007b] and *Whittaker et al.* [2008] demonstrated that rivers crossing active faults in Italy had knickzones that related to a mid-Pleistocene increase in fault throw rate, showed that the vertical height of knickzones upstream of faults scaled with fault displacement, and argued that the landscape response time to active faulting was between 1 and 3 million years for bedrock channels with drainage areas <70 km$^2$ eroding hard limestone. These studies also showed that channel narrowing played a major role in helping channels cut across active faults by increasing bed shear stress.

[4] The stream power erosion law, which treats fluvial erosion rate as a power law function of both upstream contributing drainage area, $A$, and channel gradient, $S$, provides one theoretical context for understanding the longer-term knickzone evolution in bedrock channels [*Tucker and Whipple*, 2002; *Whipple and Tucker*, 2002; *Crosby and Whipple*, 2006; *Whittaker et al.*, 2008]. Stream power erosion laws typically have the form

$$\frac{dZ}{dt} = U - f(Q_s)K\frac{A^m}{W}S^n, \qquad (1)$$

where the rate of change of elevation, $Z$, with time, $t$, depends on the imposed uplift rate, $U$, and on a power law function of drainage area, $A$ (as a proxy for catchment discharge), channel width, $W$, and downstream channel slope, $S$. $m$ and $n$ are positive exponents that describe the relative dependency of stream erosion rates on $A$ and $S$, $f(Q_s)$ is a term that describes sediment supply effects on fluvial erosion rate, and $K$ is a parameter describing erosional efficiency. $W$ may be described as a power law function of $A$ (and is often taken to scale with $\sqrt{A}$) [*Whittaker et al.*, 2007a, 2007b], in which case its effect can be subsumed into exponent $m$ and coefficient $K$ [e.g., *Attal et al.*, 2008], and $f(Q_s)$ is often taken to be equal to 1 [cf. *Cowie et al.*, 2008]. While not dealing explicitly with the physics of knickpoint retreat, it is well established that the solution to any standard form of the stream power erosion law is a nonlinear kinematic wave, which has an intrinsic wave celerity that can be taken to represent a knickpoint retreat rate [*Tucker and Whipple*, 2002; *Whipple and Tucker*, 2002; *Wobus et al.*, 2006a, 2006b; *Whittaker et al.*, 2008]. This can be approximated simply by

$$C_E \sim \Psi_K A^m S^{n-1}, \qquad (2)$$

where $\Psi_K$ is a parameter that implicitly represents all other controls on wave celerity (including $K$, which embeds lithology and width effects) and whose dimensions are dependent on the stream power exponents $m$ and $n$ [e.g. *Tucker and Whipple*, 2002; *Whittaker et al.*, 2008]. For a unit stream power erosion model, where erosion rate is dependent on the rate of energy expenditure per unit width, and subsuming $W$ scaling within the exponent on $A$ [cf. *Whittaker et al.*, 2007a], then $m = 0.5$, $n = 1$ in equation (1), and $C_E$ should be a function of the square root of drainage area [*Tucker and Whipple*, 2002; *Whittaker et al.*, 2008]. Geometric derivations using normalized steepness indices also produce similar conclusions [e.g., *Wobus et al.*, 2006b].

[5] However, relatively few field studies have focused explicitly on the factors that control plan view knickzone or knickpoint retreat rates to well-constrained base-level perturbations over longer timescales (i.e., $10^4$–$10^6$ years) within this context. *Bishop et al.* [2005] demonstrated that knickpoint retreat rates scale with catchment area for isostatically uplifted rivers in eastern Scotland, although they lacked detailed constraints on the timing and rate of base level change, so their data are not sufficient to demonstrate unambiguously that retreat rates are consistent with a unit stream power model. Similarly, *Harkins et al.* [2007] argued that the Yellow River, draining the Tibetan plateau, is undergoing a transient response to relative base-level change and the documented long profile convexities (i.e., knickzones) have elevated erosion rates that are best explained in the context of

knickpoint migration as a kinematic rather than diffusive wave. However, the authors were unable to identify the timing and duration of the downstream base-level fall that led to knickzone formation. *Crosby and Whipple* [2006] investigated knickpoint distribution in the Waipaoa River, New Zealand, following a base-level fall at ∼18 ka. However, based upon their data they could not discriminate between either knickpoint migration since base-level fall being the result of a simple power law function of drainage area, or the knickpoints lying at a low threshold drainage area, below which the channel could not incise. *Berlin and Anderson* [2007] also considered knickpoint migration within the context of a unit stream power erosion law, and neatly showed that channels draining the Roan Plateau, Colorado, had knickpoints that were retreating at a rate approximately proportional to the square root of catchment drainage area. However, the timing and magnitude of base level fall were again not well constrained, which resulted in an explicit trade-off between the constant of proportionality in best fit model solutions for wave celerity and the predicted knickpoint initiation time. Recently, *Jansen et al.* [2011] proposed that in addition to drainage area or discharge, sediment supply in the form of a "tools" effect likely modulated Holocene knickpoint retreat rates in response to glacio-isostatic base level fall in Scotland, using cosmogenically derived strath terrace ages. However, the authors did not have enough constraints to quantify explicitly these sediment supply effects within a general stream power erosion law [cf. *Gasparini et al.*, 2006].

[6] These studies therefore all highlight the need to quantify rates of knickpoint retreat in response to a relative base-level adjustment in a setting where the timing and magnitude of the perturbation are known, and where the long-term erosional dynamics of the system (for example, near the detachment-limited end-member) are already well constrained. In this paper we address this important problem. We compare two well-constrained field examples of bedrock rivers that have previously been characterized by stream power erosion law behavior, which are undergoing a well-documented transient response to active normal faulting in southern Turkey and central Italy [*Whittaker et al.*, 2007b; *Whittaker et al.*, 2008; *Boulton and Whittaker*, 2009; *Whittaker et al.*, 2010]. These channels have clearly documented long profile convexities and an initial analysis for selected Italian catchments [*Whittaker et al.*, 2008] suggested that some of these knickzones had retreated more rapidly upstream from faults which were slipping faster. However, this study was unable to identify unambiguously the cause or mechanism for this.

[7] We therefore use published data and field observations of the rate and timing of faulting, dominant channel erosion process and climate history in the two areas (section 2) as boundary conditions to derive new constraints on the factors that control knickpoint retreat. We derive the rate of knickpoint retreat for channels in each area, corrected for the distribution of drainage area with catchment length, and we measure Selby rock mass strength for each field site (section 3). We subsequently compare the extent to which differences in knickpoint retreat rate are controlled by (i) lithology; (ii) variations in fault throw rate; and (iii) location in either Turkey or Italy (section 4). Finally, we evaluate whether differences in tectonic rate, climate or fluvial erosional dynamics account for our results (section 5).

## 2. Study Areas

### 2.1. Hatay Graben, Southern Turkey

[8] The Hatay Graben is a Plio-Quaternary basin [*Boulton et al.*, 2006; *Boulton and Robertson*, 2008] located in south-central Turkey adjacent to the northern part of the Dead Sea Fault Zone (DSFZ; inset Figure 1). The graben is orientated NE-SW and is 20 km wide and ∼50 km in length. The asymmetric topography of the graben is controlled by large en-echelon normal faults on the SE margin of the basin [*Boulton and Robertson*, 2008; *Boulton and Whittaker*, 2009]. The southern footwall of the graben is dominated by Palaeogene and Middle Miocene bioclastic limestones, while the hanging wall is filled with syntectonic Pliocene to Recent siltstones, sandstones and conglomerates indicative of coastal and fluvial environments (Figure 1a) [*Boulton et al.*, 2006, 2007; *Boulton and Robertson*, 2007]. The area (from 35.9°N to 36.75°N, 35.76°E to 36.7°E) has experienced at least 35 earthquakes with a body wave magnitude ≤5.7 in the past 20 years (USGS National Earthquake Information Center, http://earthquake.usgs.gov/regional/neic/). Focal plane mechanisms of recent shallow earthquakes suggest the faults to be extensional dip-slip to oblique-slip in nature [*Erdik et al.*, 1997; *Över et al.*, 2002; Harvard CMT catalog]. The fault set bounding the southern margin of the graben has been active since at least the Early Pliocene and has a Pliocene to Recent maximum throw of 1000 ± 50 m east of the city of Antakya [*Boulton et al.*, 2006; *Boulton and Whittaker*, 2009].

[9] A number of small bedrock rivers with drainage areas between 10 and 40 km² cross these basin bounding active faults (Figure 1b). These rivers have convex-up long profiles, with knickzones 1–3 km upstream of the basin-bounding normal fault, where the channels steepen and actively incise the bedrock substrate, leading to localized gorge formation [*Boulton and Whittaker*, 2009] (Figures 2a and 2b). These small rivers carry little bed load sediment, show limited to absent sediment cover on the bed and show morphologies consistent with bedrock erosion by plucking and abrasion [*Boulton and Whittaker*, 2009]. The positions of these knickpoints do not correlate with any lithological boundaries, nor are they located at a single threshold drainage area. Moreover, both the total throw of the basin-bounding fault, and the vertical elevation of the knickpoints as measured upstream from the fault, are correlated and vary systematically along strike [*Boulton and Whittaker*, 2009]. Consequently they have been explained as an ongoing transient response of the fluvial system to a tectonic perturbation [cf. *Wobus et al.*, 2006a; *Whittaker et al.*, 2007a, 2008; *Boulton and Whittaker*, 2009] (Figure 2c).

[10] *Boulton and Whittaker* [2009] used a synthesis of geological and geomorphic mapping [*Boulton et al.*, 2006]; stratigraphic observations of sediment thickness and age [*Boulton and Robertson*, 2007, 2008]; measurements of fault displacement; observations of fault strand length; and calculations based on how fault slip rates are predicted to evolve as fault tips link from fault interaction theory [e.g., *Cowie and Roberts*, 2001] to demonstrate that the normal faults
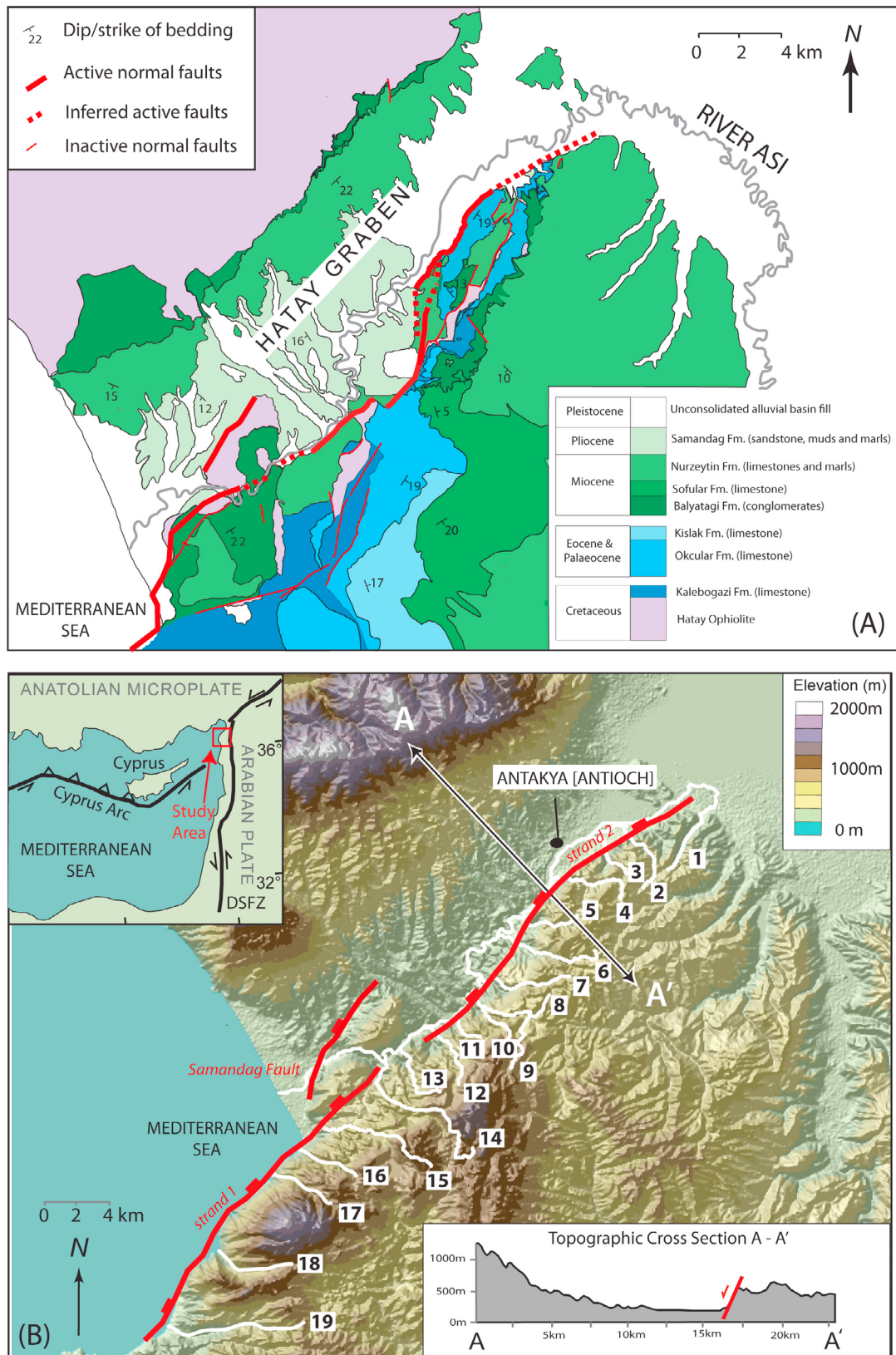
**Figure 1.** (a) Geological map of the Hatay Graben, Turkey, simplified from *Boulton and Whittaker* [2009]. Thick red lines show mapped normal faults. (b) Topographic map showing locations of the river catchments in this study. Upper left inset shows the location of the Hatay Graben within the Eastern Mediterranean; lower left inset shows the topographic profile through the graben along the line A–A′. Thick red lines show the active fault strands deduced in *Boulton and Whittaker* [2009].
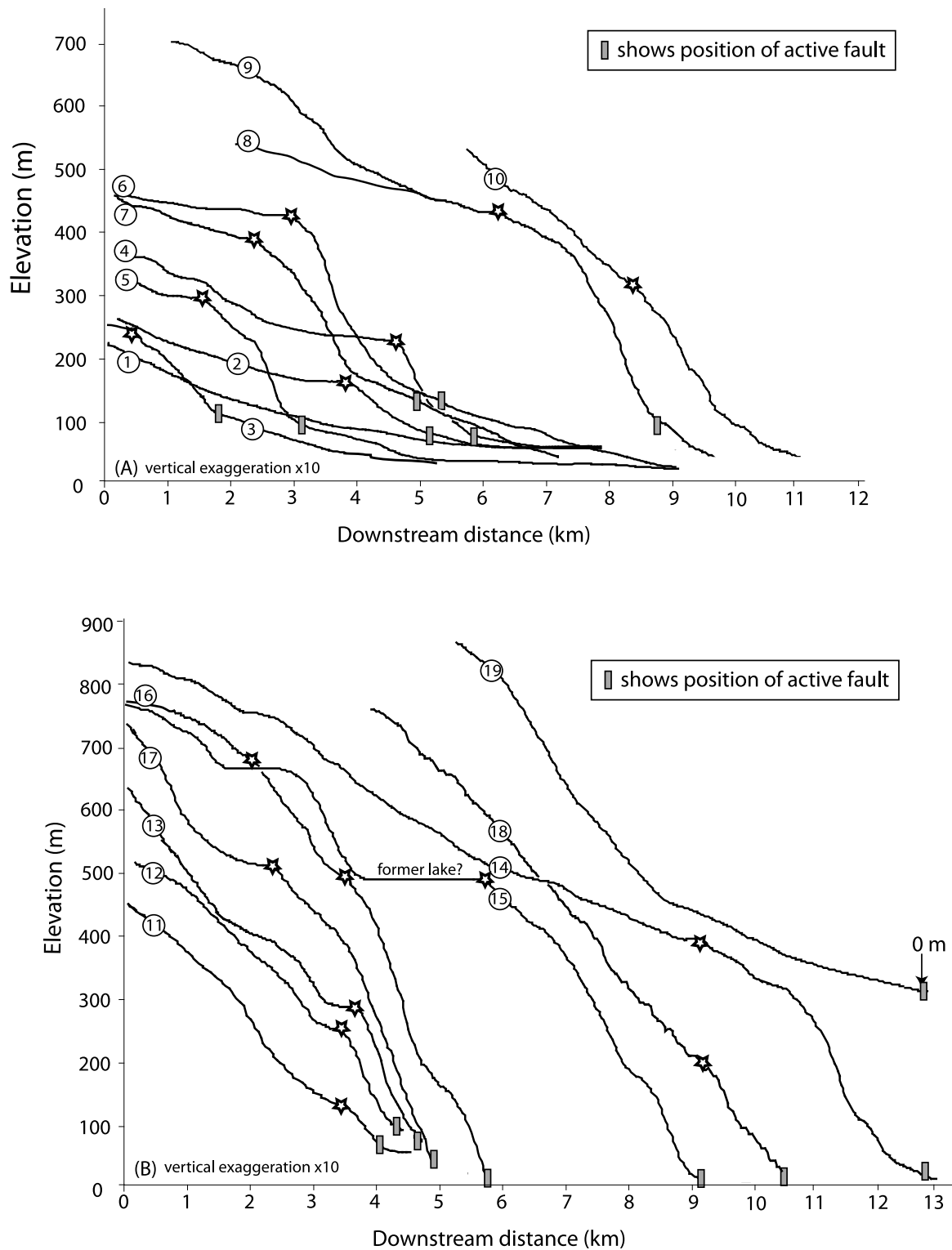
**Figure 2.** Long profiles of rivers crossing active normal faults in the Hatay Graben, Turkey, adapted from *Boulton and Whittaker* [2009]. Catchment locations are shown in Figure 1. The location where the river intersects the fault is shown; catchment details are listed in Table 1. Fault throw rate increased due to linkage at ~1.4 Ma; stars show present-day location of knickpoints generated by this tectonic perturbation. (a) Rivers crossing the northeastern fault strand 2; (b) rivers crossing the southwestern fault strand 1. Two profiles have been shifted along the *x* axis (18) and additionally up the *y* axis (19) to make the shape of the long profile as clear as possible and to reduce profile intersections. Knickpoints are shown as stars and represent the maximum rate of change of slope upstream for the long profile smoothed using a high order polynomial fit.

bounding the southern margin of the basin form two linked strands, each of length ~25 km. Their calculations showed that fault linkage occurred at 1.4 ± 0.2 Ma and that the graben bounding faults increased their throw rate as a result of this interaction by a factor of at least four; this geologically instantaneous increase in relative uplift rate is responsible for the knickpoint initiation and the ongoing transient fluvial response in the Hatay Graben. The normal faults now have a present-day maximum throw rate of 0.4–0.5 mm/yr and this slip rate decays toward the tips of each of the two strands in a predictable manner [*Boulton and Whittaker*, 2009].

[11] A range of Quaternary palaeo-climate proxy data for the Hatay graben and the Levantine coast of the Eastern Mediterranean has recently been synthesized by *Robinson et al.* [2006]. These records, consistent with global climate model (GCM) reconstructions, argue for a cooler, arid climate during glacial periods, although winter temperatures of 2–4°C at the LGM do not suggest pervasive frozen ground conditions during glacial stages. In particular, elevated non-arboreal pollen values for the Gharb Valley, ~50 km south of Antakya, suggest the presence of extremely arid conditions during glacial periods, with some phases such as the Younger Dryas dominated by *Chenopodiacae*, flowering plants now only found in areas with less than 100 mm/y annual rainfall [cf. *Rossignol-Strick*, 1995; *Meadows*, 2005]. These observations of enhanced aridity are supported by lake level reconstructions, analysis of calcretes and speleothem cave data for localities further south on the Levantine coast [*Robinson et al.*, 2006]. *Bar-Matthews et al.* [1997, 2003] quantify palaeo-rainfall based on $\delta^{18}O$ values from speleothems in northern Israel. For the LGM, they estimated a mean annual rainfall of 250–400 mm at the Soreq Cave site [*Bar-Matthews et al.*, 1997], representing 50–80% of present-day rainfall (500 mmyr$^{-1}$). Their results also indicate that the mean annual precipitation between 7000 yrs and ~500 yrs ago was less than at the present time [*Bar-Matthews et al.*, 2003]. In general, the proxy data and GCM reconstructions suggest that long-term total annual rainfall on the Levantine coast may have been lower by a factor of approximately two during glacial periods in the last million years [*Robinson et al.*, 2006], with additional phases of extreme aridity. Seasonality in precipitation remained significant, with negligible summer rainfall, suggesting no fluvial transport except for the winter months.

[12] We exploit these existing constraints on the palaeo-climate and on the timing and magnitude of the tectonic perturbation to provide a good field template to evaluate how the rate of knickzone retreat varies between catchments of different size, and also with different slip rates within the semi-arid climate of southern Turkey.

## 2.2. Central Apennines, Italy

[13] The fault array of the central Apennines, Italy, is one of the best constrained areas of normal faulting in the world [*Cowie and Roberts*, 2001; *Roberts and Michetti*, 2004; *Whittaker et al.*, 2008]. The Apennines originated as a NE-verging imbricate fold and thrust belt that formed as a result of convergence between the Eurasian and African plates [e.g., *D'Agostino et al.*, 2001; *Roberts and Michetti*, 2004]. Concurrent with thrusting, a zone of extension formed behind the compressional front, driven by roll-back of the Calabrian subduction zone [*Lavecchia et al.*, 1994;

*D'Agostino et al.*, 2001]. As a result, a network of SE-NW-striking normal faults has developed that accommodates stretching of up to 6 mm/yr across Italy [*Roberts and Michetti*, 2004] (Figure 3a). Uplifted footwalls contain Mesozoic platform carbonates, while the associated hanging wall basins are filled by fluvial and lacustrine continental deposits from the Late Pliocene to Recent [*Cavinato and DeCelles*, 1999; *Cavinato et al.*, 2002] (Figure 3a). Fault throws and throw rates have been calculated from the Late Pliocene to Present from integrated seismic and borehole surveys [*Cavinato et al.*, 2002], trenching work [e.g., *Pantosti et al.*, 1996], offsets of geological marker beds and the height of post-glacial fault scarps [e.g., *Roberts and Michetti*, 2004] and cosmogenic dating of such scarps [e.g., *Palumbo et al.*, 2004]. Throw and throw rate vary across the array, with the largest values for faults near the center of the array. Slip rates <0.4 mm/yr are documented for faults at the north and south edges of the array (e.g., Leonessa and S. Cassino faults). It is also known that slip rates on many of the centrally located faults have varied through time as a result of fault growth and interaction [*Cowie and Roberts*, 2001; *Roberts and Michetti*, 2004; *Whittaker et al.*, 2008] (Figure 3a, red). Geological observations, seismic surveys and numerical modeling show that this slip-rate increase occurred at ~0.8 Ma for the centrally located faults, while distal faults have moved at a constant rate for 3 My [*Cowie and Roberts*, 2001; *Roberts and Michetti*, 2004].

[14] In addition to excellent structural controls, much is known about the climatic changes experienced in the region during the Quaternary. Estimates of the prevailing mean annual rainfall and ground conditions for glacial periods come from observations of palaeo-lake levels [*Giraudi*, 1989; *Giraudi and Frezzotti*, 1997]; palynology and palaeo-environmental reconstructions [*Ramrath et al.*, 1999; *Allen et al.*, 2000]; measurements of the extent and oxygen isotopic composition of corrie glaciers in the Gran Sasso [*Giraudi and Frezzotti*, 1997]; and sedimentological considerations. Data show that the level of the Fucino lake location (Figure 3) was several tens of meters higher both before and during the LGM than in the Holocene, with peak glacial advances being directly correlated with elevated lake levels [*Giraudi*, 1989; *Giraudi and Frezzotti*, 1997]. Analysis of sediment cores from ~30 ka to present for the Lago di Mezzano and Lago Grande di Monticchio (which lie to the north and south of the study area, respectively) are consistent with a regionally significant cold and wet phase from 30 ka to 23.5 ka [*Ramrath et al.*, 1999], although precipitation was probably lowered at the LGM peak by ~20% [*Jost et al.*, 2005]. Hydrological models for the Po River, northern Apennines, also support increased run-off throughout this time period driven by spring melt of glaciers [*Kettner and Syvitski*, 2008]. Moreover, sharply decreased infiltration due to the periglacial frozen ground conditions in the underlying carbonate bedrock has also been suggested during these glacial periods [*Giraudi and Frezzotti*, 1997; *Bogaart et al.*, 2003; *Tucker et al.*, 2011], with the mean temperature of the coldest month being <−10°C at the LGM [*Allen et al.*, 2000]. These frozen ground conditions would have significantly boosted run-off. Fluvial conglomerates dated or attributed to previous glacial stages are also abundant in the central Apennines, and the coarse calibre of the clasts ($D_{50}$ up to 20 cm) clearly testifies to the enhanced transport
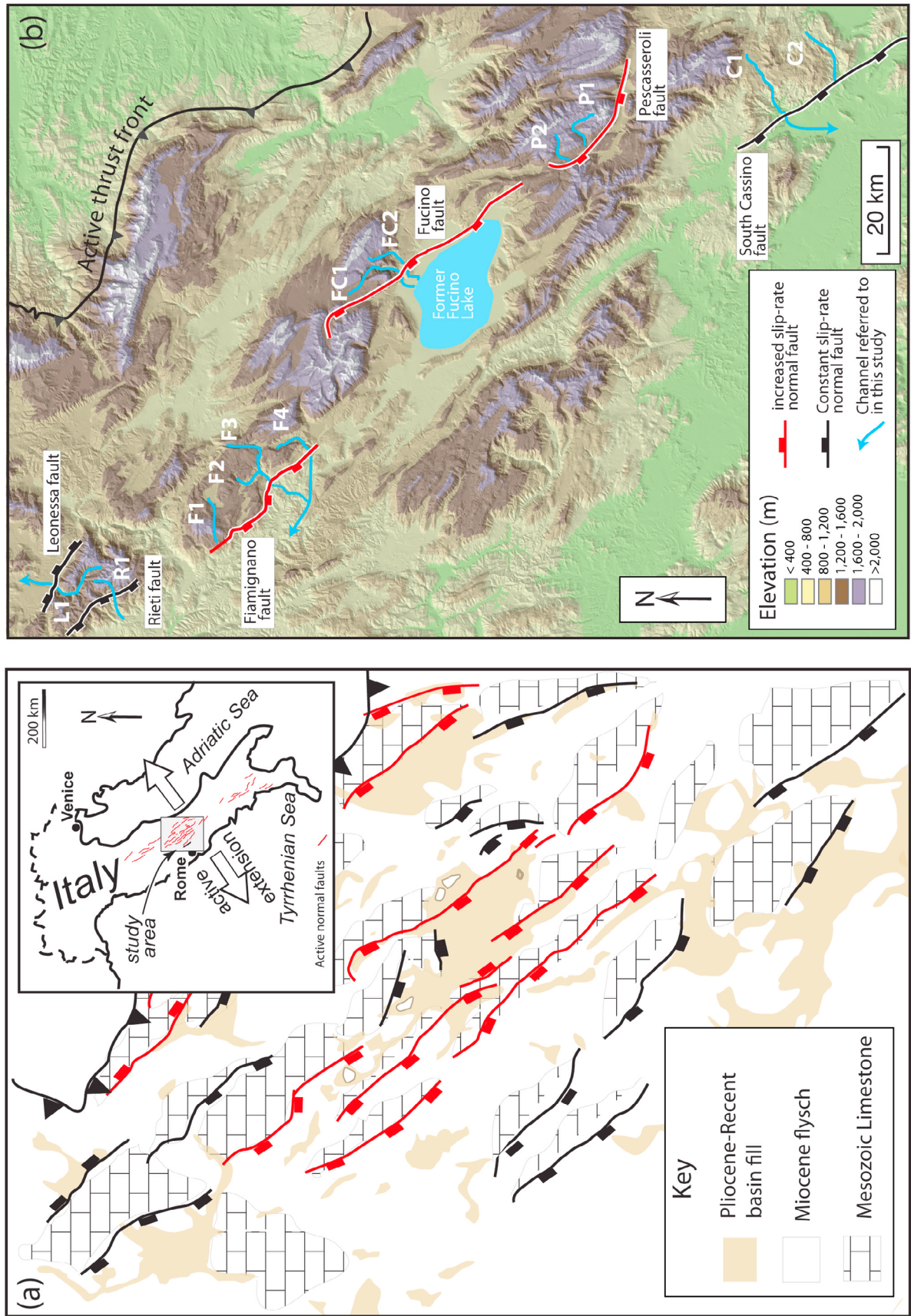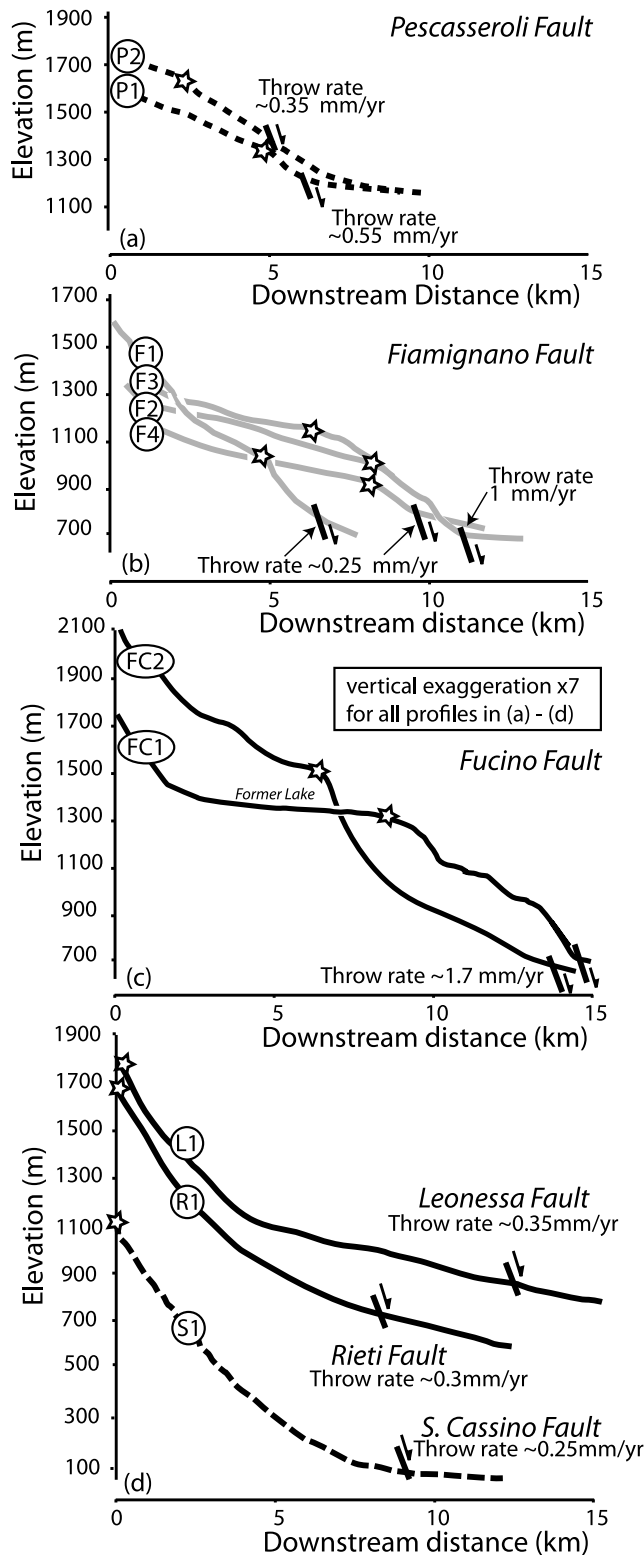
**Figure 3.** (a) Structural and lithologic map of the central Apennines. Inset shows study location within Italy. Normal faults that are known to have increased their slip rate at ~0.8 Ma are highlighted in red. (b) Topographic map of central Apennines, showing locations of the river catchments in this study.

capacity of small mountain rivers during glacial periods compared to the present day, where $D_{50}$ is typically 5–10 cm [*Wegmann and Pazzaglia*, 2009; *Whittaker et al.*, 2010]. These observations imply that run-off could have been enhanced by a factor of 2–4 in Apennine rivers for past glacial periods in the last 1 My, relative to the present interglacial.



**Figure 4.** Long profiles of rivers crossing active normal faults in the central Apennines, adapted from *Whittaker et al.* [2008]. Catchment locations are shown in Figure 3. Estimates of throw rate where the river intersects the fault are shown in each case; catchment details are listed in Table 1. Fault throw rate increased due to linkage at ~0.8 Ma; stars show present-day location of knickpoints generated by this tectonic perturbation. (a) Rivers crossing the Pescasseroli fault; (b) rivers crossing the Fiamignano fault; (c) rivers crossing the Fucino fault; (d) rivers crossing active faults that have slipped at a constant rate for 3 My but which have now reached topographic steady state. Knickpoints are shown as stars and represent the maximum rate of change of slope upstream for the long profile smoothed using a high order polynomial fit.

[15] Due to these excellent climatic and tectonic constraints, the central Apennines have been an area of considerable geomorphic study in recent years, summarized briefly below. The bedrock rivers in the area are highly starved of sediment, often with <40% coverage of sediment on the bed [*Whittaker et al.*, 2007b; *Cowie et al.*, 2008], and those draining across the increased slip-rate normal faults show the presence of large knickzones upstream of the active faults (Figures 4a–4c). This landscape response is associated with narrowed channel and valley widths, rejuvenated hill slopes and migration of the drainage divide toward the fault [*Whittaker et al.*, 2007a, 2008]. It is now widely accepted that these rivers are undergoing a transient response to the onset of fault interaction and accompanying increase in slip rate at 0.8 Ma documented above [*Whittaker et al.*, 2007a, 2007b, 2008; *Attal et al.*, 2008; *Tucker*, 2009; *Whittaker et al.*, 2010]. Field and modeling studies both argue that the incision of these rivers across the uplifted normal fault blocks can be adequately described with a unit stream power model for catchment erosion, so the rivers must lie close to the detachment limited end-member [*Whittaker et al.*, 2007a; *Cowie et al.*, 2008; *Attal et al.*, 2008]. This conclusion is supported by derivations of Shields stress values from measurements of grain size in the channel where present, which are up to two orders of magnitude greater than the threshold value for transport-limited gravel bed systems [*Whittaker et al.*, 2007b]. By contrast, rivers that cut across faults that have moved at a constant rate for the past 3 My have concave-up long profiles and do not display these transient characteristics [*Whittaker et al.*, 2007b, 2008] (Figure 4d). A comparison of unit stream power driven erosivity downsystem with reconstructions of footwall uplift has suggested that these catchments have now reached topographic steady state [*Whittaker et al.*, 2007b].

[16] In this study, we use this existing work in Italy as a well-constrained template to (i) investigate the controls on the rates of knickzone migration for bedrock rivers close to the detachment-limited end-member undergoing a transient response to a known tectonic perturbation and (ii) as a contrasting data set to the Turkish examples outlined in section 5.1.

## 3. Approach and Methodology

[17] The two field data sets offer an excellent opportunity to quantify and compare the long-term migration rate of

knickpoints for well-studied river systems near the detachment-limited end-member, crossing a range of lithological types in two different climate zones, and to evaluate the dominant controls on knickpoint retreat rate. We make the reasonable assumption that the top of the convex reach upstream of the active faults in each of the long profiles (i.e., the knickpoint) represents the distance upstream that the transient wave-like response to tectonic perturbation has propagated [cf. *Crosby and Whipple*, 2006; *Whittaker et al.*, 2007b, 2008; *Berlin and Anderson*, 2009; *Attal et al.*, 2011]. We identify the knickpoint as the maximum rate of change of slope from the long profiles in Figures 2 and 4 (stars indicate knickpoints); the locations of knickpoints and knickzones were additionally ground-truthed by field reconnaissance to verify our DEM interpretation [cf. *Whittaker et al.*, 2007b, 2008; *Boulton and Whittaker*, 2009]. The average knickpoint migration rate was determined by measuring the upstream distance to the knickpoint from the mapped position of the normal fault, and dividing this distance by the time since the documented fault slip rate increase [cf. *Bishop et al.*, 2005; *Berlin and Anderson*, 2007; *Jansen et al.*, 2011]. For the Turkish examples, we use a conservative range for the timing of the fault linkage event of 1.2 to 1.6 Ma, consistent with the range of values deduced by *Boulton and Whittaker* [2009]. For the timing of fault interaction in the Italian examples, we use 0.7 to 1 Ma [*Cowie and Roberts*, 2001; *Whittaker et al.*, 2008]. For comparative purposes we also include in the analysis Italian bedrock rivers, similar in size to the other studied channels, crossing faults that have slipped at a constant rate for the past 3 Ma, which have now reached topographic steady state (section 2.2). These channels were perturbed by the initiation of active faulting at 3 Ma, but because response times in Italy are shorter than this time period [*Whittaker et al.*, 2007a, 2007b], any knickpoint that formed when the faults initiated in the Late Pliocene has already migrated through the catchment to the headwaters [*Whittaker et al.*, 2007b]. A conservative minimum estimate of the time required for this to happen can be gained by dividing the catchment length by the time since the initiation of faulting; maximum values are obtained using the calculation of *Whittaker et al.* [2007b], which proposes that the fluvial landscape response time is likely to be ~2 My. These equivalent rates are important to test whether the Italian data sets for rivers crossing faults with different slip rate histories are self-consistent.

[18] These average rates conceal differences in catchment size and lithology which are the most widely acknowledged controls on knickpoint migration rates (as discussed in section 1) [see also *Bishop et al.*, 2005; *Crosby and Whipple*, 2006; *Wobus et al.*, 2006a, 2006b; *Berlin and Anderson*, 2007]. The Italian and Turkish catchments are bedrock catchments that have both been adequately described by a unit stream power law (as discussed in section 2) [see also *Whittaker et al.*, 2007b; *Boulton and Whittaker*, 2009]. Following *Whittaker et al.* [2008], we therefore normalize the knickpoint retreat rates by $\sqrt{A}$ to evaluate explicitly whether catchment size accounts for the differences in knickpoint migration between channels at the two field sites, to obtain a catchment area independent measure of knickpoint retreat rate, $\Psi_A$, where $\Psi_A = \Psi_K S^{n-1}$ and $\Psi_A = \Psi_K$ for $n = 1$ (equation (2)) However, it is not simply the total drainage area at the fault that controls knickpoint retreat, it is the

*distribution* of drainage area upstream of the knickzone that matters; consequently the upstream rate of drainage area reduction determines the rate of change of knickpoint retreat rate. We therefore iteratively calculate the celerity of knickpoint retreat, $C_E$ (equation (2)) as a function of the known decline in the square root of drainage area with decreasing upstream distance, $\sqrt{A_{f(L)}}$ as extracted from each catchment DEM as

$$C_E = \Psi_A \sqrt{A_{f(L)}}. \tag{3}$$

In all cases $A$ and $L$ come from the DEM-derived catchments presented by *Whittaker et al.* [2008] and *Boulton and Whittaker* [2009]. To determine a value of the parameter $\Psi_A$ that reproduces the documented plan view position of the knickpoint, $x_{knick}$ within the catchment we use

$$x_{knick} = x_{fault} - \left(\Psi_A \sqrt{A_{f(L)}}\right)t, \tag{4}$$

where $x_{fault}$ is the downstream position of the fault, and $t$ is the total time since the slip rate increase. This calculation allows for the knickzone migration rate to slow upstream over time, as the square root of drainage area declines upstream [cf. *Berlin and Anderson*, 2007; *Whittaker et al.*, 2008]. If $A$ is the main control on the velocity of knickzone migration, and hence on the landscape response time to tectonic perturbation, then we expect $\Psi_A$ to be approximately the same for all channels. In this case, fluvial response times for comparable catchments that differ in size only would be identical, if they also obeyed similar scaling ($L \sim \sqrt{A}$) between channel length and drainage area (Hack's Law). Full details of the studied channels are shown in Table 1. While other workers have allowed the power law exponent, $m$, on $A$ in equations (1) and (2) to vary [e.g., *Crosby and Whipple*, 2006; *Berlin and Anderson*, 2007], we are less keen on such an approach here, because it risks normalizing the field-derived rates by an arbitrary value that is neither theoretically explained, nor justified by previously published work in the field areas under study (section 2). We therefore normalize using $m = 0.5$ in the first instance. However, we also use field measurements of mean channel width within the knickzones (Table 1) to test whether our $\Psi_A$ calculations are affected by channel narrowing where rivers cut across active faults (see section 5.3) [cf. *Whittaker et al.*, 2007a].

[19] While a standard unit stream power model suggests that it is $A$ and not $S$ that determines knickzone retreat rates, if the transient tectonic perturbation is large or if $n \neq 1$ then channel gradient will moderate the rate of knickpoint retreat (equation (2)) [e.g., *Wobus et al.*, 2006b]. If $n > 1$, the knickpoint will retreat faster on steeper slopes for the same drainage area, while if $n < 1$, the reverse is true [*Tucker and Whipple*, 2002; *Whipple and Tucker*, 2002]. Therefore, we present the knickpoint retreat rate parameter, $\Psi_A$, as a function of tectonic throw rate in both field areas, using this large data set to test initial observations that from Italy that knickpoint retreat rates for some bedrock channels are sensitive to fault displacement rate, potentially because channel slopes are higher upstream of faster slipping faults [cf. *Cowie et al.*, 2008; *Whittaker et al.*, 2008]. Effective fault throw rates for each channel are shown in Table 1, and are taken from the summary data presented in *Whittaker et al.* [2008] in

**Table 1.** Field Data and Knickpoint Retreat Rates for Study Channels

| River | Distance to Fault (km) | Distance to Knickpoint (km) | Drainage Area (km²) | Fault Throw Rate[a] (mm/yr) | Maximum Knickpoint Retreat Rate (mm/yr) | Minimum Knickpoint Retreat Rate (mm/yr) | Max $\psi$A (1/yr) | Min $\psi$A (1/yr) | Channel Width[b] (m) | Channel Slope[c] (m/m) |
|---|---|---|---|---|---|---|---|---|---|---|
| | | | | *Turkey* | | | | | | |
| 1 | 9.8 | n/a | 9.9 | 0.00 | n/a | n/a | n/a | n/a | n/a | n/a |
| 2 | 7.9 | 1.4 | 9.8 | 0.10 | 1.12 | 0.88 | 3.22E–07 | 2.52E–07 | 8–10 | 0.03 |
| 3 | 5.4 | 1.3 | 6.3 | 0.15 | 1.08 | 0.81 | 3.82E–07 | 2.96E–07 | 8–10 | 0.1 |
| 4 | 8.3 | 1.3 | 10.2 | 0.20 | 1.08 | 0.81 | 3.05E–07 | 2.29E–07 | 8–10 | 0.15 |
| 5 | 5.3 | 1.5 | 6.9 | 0.30 | 1.25 | 0.94 | 4.28E–07 | 3.21E–07 | 8–10 | 0.13 |
| 6 | 9.0 | 2.3 | 12.8 | 0.35 | 1.92 | 1.44 | 4.82E–07 | 3.62E–07 | 8–10 | 0.17 |
| 7 | 7.6 | 2.4 | 9.8 | 0.40 | 2.00 | 1.50 | 5.75E–07 | 4.31E–07 | 8–10 | 0.13 |
| 8 | 7.1 | 1.9 | 14.8 | 0.45 | 1.58 | 1.19 | 3.70E–07 | 2.78E–07 | 8–10 | 0.1 |
| 9 | 10.1 | 1.9 | 14.8 | 0.45 | 1.58 | 1.19 | 3.70E–07 | 2.78E–07 | 8–10 | 0.1 |
| 10 | 5.2 | 1.8 | 8.1 | 0.30 | 1.50 | 1.13 | 4.74E–07 | 3.56E–07 | 8–10 | 0.13 |
| 11 | 4.2 | 0.4 | 5.0 | 0.20 | 0.33 | 0.25 | 1.34E–07 | 1.01E–07 | 8–10 | 0.09 |
| 12 | 6.2 | 0.8 | 13.6 | 0.20 | 0.67 | 0.50 | 1.63E–07 | 1.22E–07 | 8–10 | 0.15 |
| 13 | 5.8 | 1.2 | 8.3 | 0.30 | 1.00 | 0.75 | 3.12E–07 | 2.34E–07 | 8–10 | 0.19 |
| 14 | 13.1 | 3.2 | 29.2 | 0.35 | 2.67 | 2.00 | 4.44E–07 | 3.33E–07 | 8–10 | 0.06 |
| 15 | 9.8 | 3.0 | 16.1 | 0.40 | 2.50 | 1.88 | 5.61E–07 | 4.81E–07 | 8–10 | 0.18 |
| 16 | 5.8 | >2 | 6.4 | 0.45 | 1.67 | 1.25 | 5.91E–07 | 4.45E–07 | 8–10 | 0.12 |
| 17 | 5.1 | 2.2 | 5.9 | 0.40 | 1.83 | 1.38 | 6.79E–07 | 5.09E–07 | 8–10 | 0.12 |
| 18 | 5.7 | 1.7 | 11.2 | 0.20 | 1.50 | 1.13 | 3.73E–07 | 3.03E–07 | 8–10 | 0.11 |
| 19 | 8.4 | n/a | 17.7 | 0.00 | n/a | n/a | n/a | n/a | n/a | n/a |
| | | | | *Italy* | | | | | | |
| L1 | 12.5 | 12.5 | 45.0 | 0.35 | 6.2 | 4.10 | 9.64E–06 | 6.43E–07 | 20 | 0.02 |
| R1 | 9.8 | 9.8 | 28.0 | 0.30 | 4.9 | 3.20 | 1.10E–06 | 7.30E–07 | 11 | 0.03 |
| S1 | 7.3 | 7.3 | 20.0 | 0.25 | 3.6 | 2.40 | 6.90E–07 | 4.60E–07 | 10 | 0.03 |
| P1 | 6.1 | 1.5 | 18.0 | 0.55 | 2.14 | 1.50 | 5.65E–07 | 4.00E–07 | 9 | 0.1 |
| P2 | 5.3 | 2.1 | 12.2 | 0.3–0.4 | 3.43 | 2.40 | 1.10E–06 | 8.09E–07 | 11 | 0.08 |
| F1 | 6.0 | 1.0 | 12.0 | 0.25 | 1.43 | 1.00 | 4.43E–07 | 3.33E–07 | n/a | 0.12 |
| F2 | 10.4 | 4.5 | 65.0 | 1.00 | 6.43 | 4.50 | 1.17E–06 | 8.62E–07 | 9 | 0.09 |
| F3 | 10.4 | 3.5 | 65.0 | 1.00 | 5.00 | 3.50 | 7.00E–07 | 5.60E–07 | 9 | 0.1 |
| F4 | 9.2 | 2.2 | 25.0 | 0.25 | 3.14 | 2.20 | 6.52E–07 | 4.90E–07 | 12 | 0.08 |
| FC1 | 11.5 | 6.0 | 41.0 | 1.75 | 8.57 | 6.00 | 1.41E–06 | 9.62E–07 | 7 | 0.14 |
| FC2 | 12.4 | 7.5 | 31.0 | 1.75 | 10.71 | 7.50 | 2.10E–06 | 1.54E–06 | 6.5 | 0.24 |

[a]Fault throw rates averaged over 1.4 My for Turkish data and averaged over 0.8 My for Italian data.

[b]Italian width data are the mean of all data in the knickzone upstream of fault or within 2 km of the knickpoint if knickzone is longer than this [*Whittaker et al.*, 2007b, 2008, 2010]. Turkish width data are estimated upstream of the active fault from field reconnaissance.

[c]Channel slope represents the average gradient within the knickzone or within 2 km of the knickpoint if the incised knickzone is longer than this.

the case of the Italian examples, and for the Hatay Graben, are taken from the along-strike distribution of fault throw rate deduced in *Boulton and Whittaker* [2009]. We also use measurements of mean channel slope within the knickzone from the available DEM data (Table 1) to evaluate how sensitive river gradient is to fault throw rate in the case that our data are consistent with $n > 1$ (see section 5.3).

[20] Lithology and rock mass strength play an important role in determining the rate and process of knickpoint retreat, directly affecting the erosion efficiency parameter, $K$, in equation (1). Therefore, typical Selby rock mass strength values (RMS) of each of the main lithological units were derived by combining measurements of the intact rock strength with field observations and measurements of the width, frequency, continuity and orientation of joints, the degree of weathering and presence or absence of groundwater flow for both study areas [*Selby*, 1980]. Weathering and structural features of the bedrock can impact greatly upon how readily the rock will erode, which a mechanical description of rock strength alone will not take into account, leading to significant overestimates of resistance to fluvial erosion in heavily jointed areas if used alone (Appendix A) [*Selby*, 1980; *Whipple et al.*, 2000].

[21] The intact compressive strength for the rock types in the study areas was measured using two methods (Appendix A). Rock strength across the Italian study area was determined in the field using a Schmidt hammer [e.g., data in *Whittaker et al.*, 2007b, 2008]. Along each river in the Italian study area, an average of twenty rebound measurements were taken at a number of sample sites, typically on fluvially abraded bedrock on the base and sides of the channel; the average of these readings was used in the determination of the RMS.

[22] Schmidt hammer measurements were not made in Turkey due to field work constraints; therefore, samples from representative lithologies from the Hatay area were subjected to load testing in the laboratory to determine the point load strength index ($I_{s(50)}$) of the samples, following the methodology outlined in the *Suggested Methods* of the International Society for Rock Mechanics [*Franklin*, 1985]. This index can be related to the uniaxial compressive strength (UCS) of the sample using the formulas derived by *Sabatakakis et al.* [2008] for a range of sedimentary lithologies (Appendix A; equations (A1)–(A4)) and those of *Diamantis et al.* [2009] for serpentinite (Appendix A, equation (A4)). The UCS value can then be used as part of the Selby RMS determination in
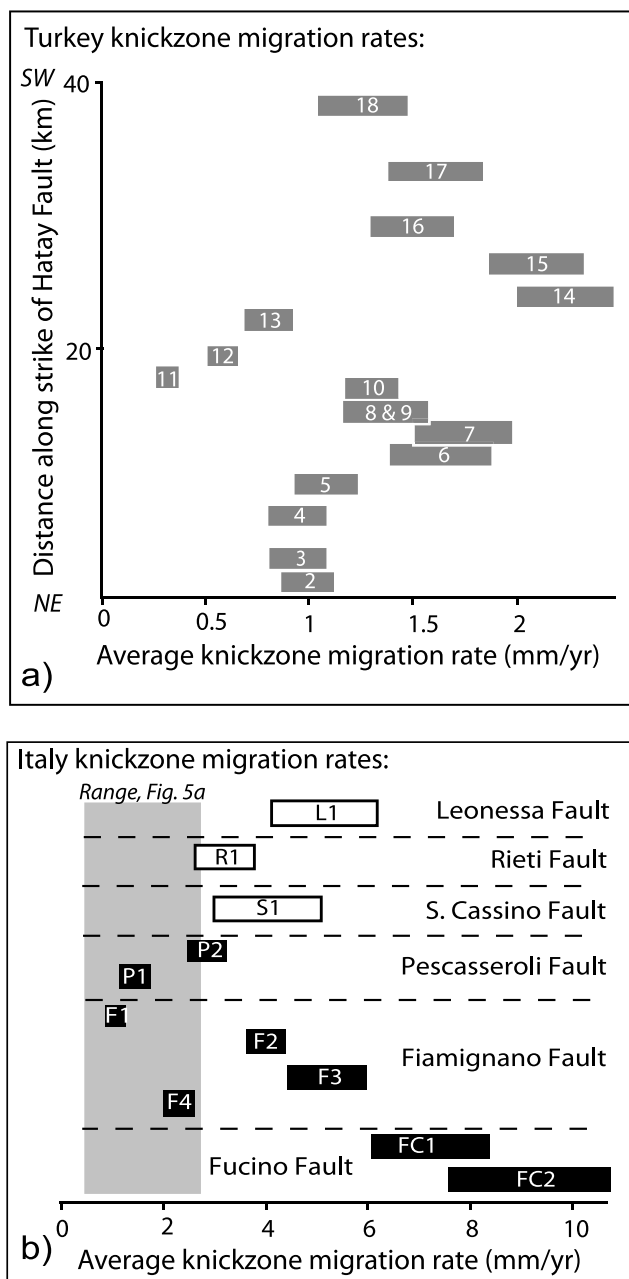
**Figure 5.** (a) Average knickpoint migration rates for the Turkish catchments shown in Figure 2 (numbered gray bars) and (b) the Italian catchments crossing active normal faults shown in Figures 4a–4c (numbered black bars). For the Turkish data, we assumed the knickpoint initiation time, $t$, was 1.2 Ma < $t$ < 1.6 Ma; and for the Italian data, we use 0.7 Ma < $t$ < 1 Ma, consistent with existing geologic constraints. White bars show inferred palaeo-knickpoint migration rate estimates for Italian catchments that cross active normal faults but which have now achieved topographic steady state. We used 2 My < $t$ < 3 My (see text).

an equivalent way to the Schmidt hammer reading. These data enable us to compare variations in rock strength between catchments, and also between study areas with differing rock types. We stress, however, that the knickpoints highlighted in Figures 2 and 4 are not located or pinned at lithological

boundaries [e.g., Figure 5b in *Whittaker et al.*, 2008; *Boulton and Whittaker*, 2009]. Therefore, these data are aimed at elucidating whether rock mass strength plays a significant role in mediating the retreat rate of knickpoints generated by a tectonic perturbation.

## 4. Results

[23] Time-averaged rates of knickzone retreat for the Turkish rivers range over an order of magnitude, from 0.2 mm/yr to >2 mm/yr (Figure 5a). These values are at least an order of magnitude slower than recent studies in Scotland where a sediment "tools" effect may be in operation [e.g., *Bishop et al.*, 2005; *Jansen et al.*, 2011], but are similar to those obtained by other workers for small catchments with drainage areas <50 km$^2$ [e.g., *Weissel and Seidl*, 1998; *Dorsey and Roering*, 2006; *Berlin and Anderson*, 2007]. However, the mean knickzone retreat rate in Turkey is lower by a factor of approximately 5 compared to the Italian data. Along the Italian channels, the transient incisional wave, developed in response to a fault slip rate increase at ∼0.8 Ma is moving at rates between 1 and 10 mm/yr (Figure 5b) [cf. *Whittaker et al.*, 2008]. It is notable that the highest knickpoint retreat rates are for catchments crossing the Fucino fault, the fastest slipping fault in the Apennines.

[24] Can these differences be explained by catchment size, or lithological variations between the catchments? Figure 6 shows the drainage-area-normalized knickpoint retreat rate parameter, $\Psi_A$, plotted against the Selby rock mass strength for the lithologies present within the knickzone of the studied rivers. $\Psi_A$ values range from $1 \times 10^{-7}$ y$^{-1}$ for relatively low slip rate faults in Turkey to >2 × 10$^{-6}$ y$^{-1}$ for higher slip rate faults in Italy, showing that even when normalized by drainage area, knickpoint retreat rates vary by more than a factor of 20 over the Turkish and Italian data sets. However, if average catchment RMS were strongly influencing knickpoint retreat rates, then we would expect to see an inverse relationship between the two parameters, i.e., the weaker the rock, the faster the knickzone would migrate and vice versa. This is not what is observed, however, with little dependence of $\Psi_A$ for our data points, which lie in the range 55 < RMS < 84. We note that in Turkey some rivers, such as 11 and 12, have low average bedrock RMS (i.e., they are easy to erode) yet also have some of the slowest rates of knickzone retreat. Furthermore, catchments 16, 17, and 18 flow in their entirety across the same Palaeogene limestone, yet the rate of knickzone retreat is different for each channel. Italian rivers have generally higher rates of knickzone retreat despite having similar rock strengths to the Turkish examples. These data are striking because they suggest that drainage-area-normalized knickpoint retreat rates are highly variable, even though they are not explainable by lithologic effects within the range of RMS values considered.

[25] Figure 7 shows the drainage-area-normalized knickpoint migration rate parameter $\Psi_A$, plotted as a function of fault slip rate in a similar way to *Whittaker et al.* [2008] (Figure 7a). Two significant results can be drawn from this graph; first, there is a noticeable dependency of $\Psi_A$, and hence the rate of knickpoint migration on the magnitude of the fault throw rate, $R$. This means that the transient wave of incision for channels crossing the high slip rate Fucino fault (slipping at 1.7 mm/yr) is moving at rates 6–7 times faster
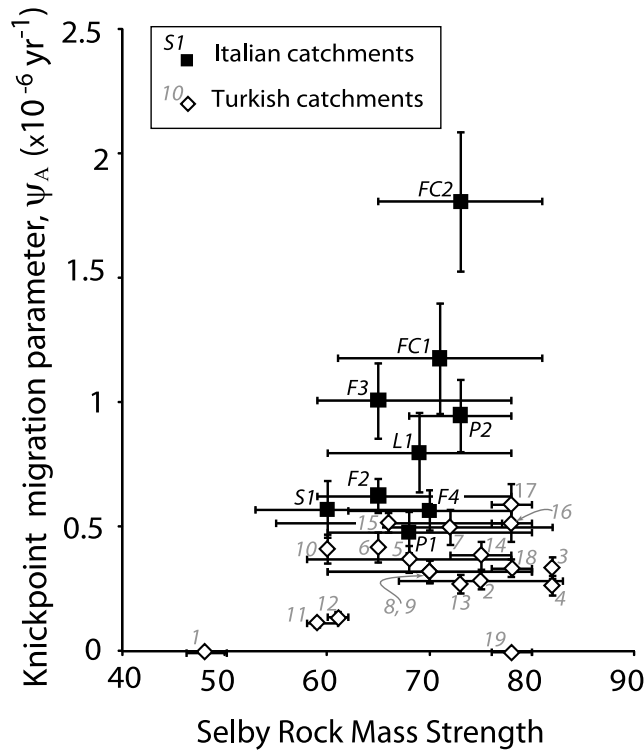
**Figure 6.** Drainage-area-normalized knickpoint migration rate parameter, $\Psi_A$, against mean Selby rock mass strength for the Turkish rivers (white diamonds) and the Italian rivers (black squares). Channels 1 and 19 with no identifiable knickzone are included for comparison. Error bars on the x axis show the range of values recorded for Selby RMS in the knickzones of the study rivers. Error bars on the y axis show the range of $\Psi_A$ values assuming the knickpoints were generated between 1.2 and 1.6 Ma for Turkey, and 0.7 and 1 Ma for Italy.

than for channels crossing faults with order of magnitude slower throw rates. This cannot be explained by drainage area variations or lithologic effects. We note that the range of palaeo-knickpoint retreat rate estimates for Italian catchments crossing active faults which are now apparently in topographic steady state (because the distribution of specific stream power down-system matches the footwall uplift profile [*Whittaker et al.*, 2007b]), is consistent with $\Psi_A$ values for other Italian rivers (Figure 7a, white bars). This relationship can be fitted with a power law of the form $\Psi_A \sim R^{0.67}$ for the Italian and Turkish data sets (Figure 7b). Regression using the minimum knickpoint migration rates, or the Italian data set alone does not significantly change the calculated exponent on R.

## 5. Discussion

### 5.1. Key Findings

[26] These data demonstrate that knickpoint retreat rates for bedrock catchments, with erosional dynamics near to the detachment-limited end-member, and undergoing a transient response to fault slip rate increase, vary significantly even when normalized for catchment size. In particular, the data

show (i) that the rate at which the transient wave of incision propagates upstream is correlated with the fault throw rate in both study areas; and (ii) that the rate is typically a factor of two greater in Italy than in Turkey for otherwise similar catchments. These differences cannot be explained simply by variations in average rock mass strength between the catchments studied. The results suggest that fault slip rates could be at least as important as differences in catchment area in setting the timescale of landscape response to tectonic perturbation, because at face value, a tenfold difference in A is predicted to produce only an approximately threefold difference in knickzone retreat rate for channels close to the detachment limited end-member, where $m \sim 0.5$ (equation (2)). In contrast, a tenfold difference in fault throw rate could produce a six- to sevenfold difference in knickzone migration rate for catchments with the same drainage area. Our results strongly suggest that fluvial response times are shorter for channels that have undergone a larger tectonic perturbation.

[27] Moreover, Figure 7 suggests that knickpoints in the Turkish catchments migrate at a slower rate than the Italian examples, even accounting for drainage area. If we compare data points for lower throw rate faults (i.e., between 0.1 and 0.5 mm/yr) in both Turkey and Italy, in order to remove the fault throw rate signal, mean $\Psi_A$ is lower for the Turkish examples than for the Italian study sites by a factor of just over 2. This implies that for identically sized catchments in Turkey and Italy that are crossing faults with similar slip rates, the celerity of the transient wave of incision, and hence the fluvial response time to tectonic perturbation, must also differ by a factor of at least two.

[28] Below we evaluate the likely explanations for the trends seen.

### 5.2. Presence of an Erosion Threshold?

[29] Modifying the stream power erosion law to include a variable critical threshold for sediment or bedrock block entrainment, $\tau_c$, below which the channel does not have enough power to incise is one way to modulate the erosional efficiency of bedrock channels [e.g., *Whipple and Tucker*, 1999; *Snyder et al.*, 2003; *Attal et al.*, 2011]. Erosion thresholds can be incorporated within a shear stress erosion law as:

$$E = k_b(\tau - \tau_c)^a, \quad (5)$$

where $\tau = \rho g H S$. $\rho$ is the density of water, $H$ represents the hydraulic radius of the channel, $k_b$ is a constant that varies between catchments, and the exponent $a$ ranges from 1 to 1.5 for typical stream power erosion "laws". The effect of a large threshold is to introduce significant nonlinear dynamics into the system because few flow events are large enough to exceed the shear stress or stream power threshold for incision [*Snyder et al.*, 2003]. Therefore, catchments governed by threshold dynamics have a longer response time to an identical perturbation than those with no, or a small, threshold. If two identical catchments reach topographic steady state with respect to an identical uplift field, the catchment governed by threshold dynamics will be steeper than the one with no effective geomorphic threshold, because increased channel gradient is needed to counter the reduction in time-integrated
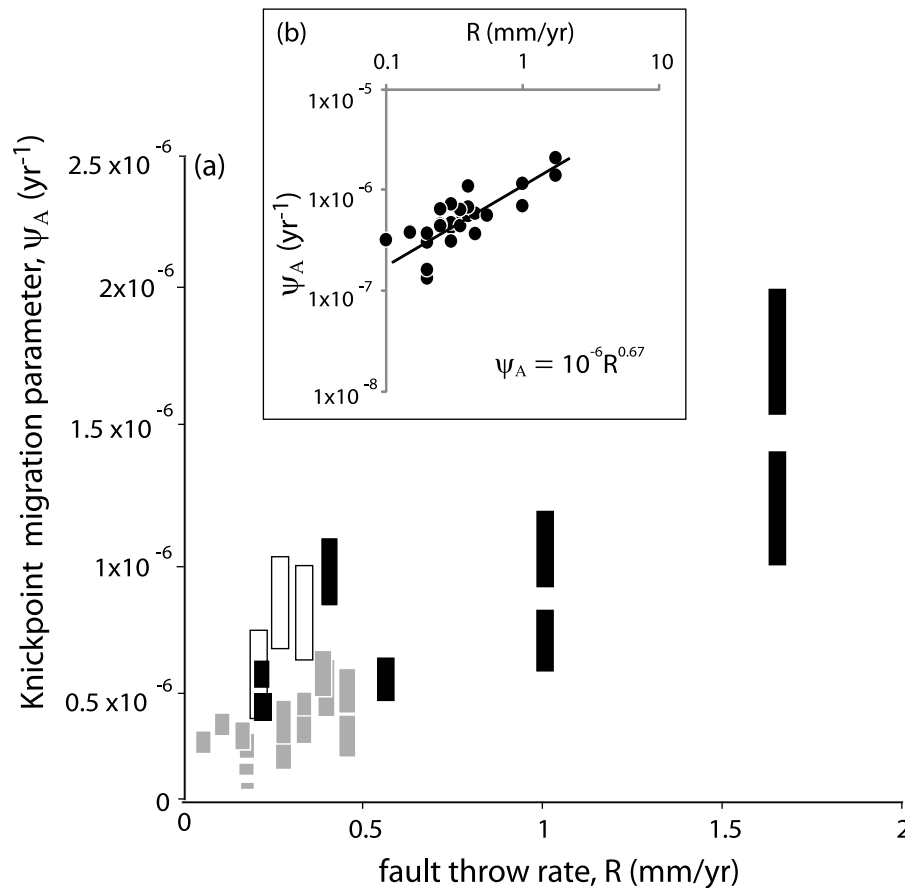
**Figure 7.** (a) Drainage-area-normalized knickpoint migration rate parameter, $\Psi_A$, against fault throw rate, $R$, for catchments in Turkey (gray bars) and Italy (black bars). Bars span range of $\Psi_A$ values for fault acceleration at 0.7–1 Ma in Italy, and 1.2–1.6 Ma in Turkey. White bars show $\Psi_A$ estimates for Italian catchments crossing active normal faults (see Figure 6). (b) Log $\Psi_A$ against log $R$ for maximum knickpoint migration rates for all channels. Line of best fit is a power law regression through the data, with the best fit equation shown.

erosivity produced by the threshold. A full treatment of these integrated dynamics requires knowledge of the time-dependent discharge distribution for each catchment [e.g., *Snyder et al.*, 2003]. In the absence of such data, we simply consider the extent to which a threshold is a plausible explanation for the trend in Figure 7, focusing on the Italian data where the channel geometry and bankfull discharge have previously been constrained [*Whittaker et al.*, 2007a, 2007b].

[30] Bed shear stresses for Italian catchments F3 (throw rate 1 mm/yr) and F4 (throw rate 0.25 mm/yr) are ~1800 and 1200 Pa at bankfull stage, respectively [see *Cowie et al.*, 2008, Figure 2]. These values correspond to bankfull discharges of 80–125 $m^3$/s [*Whittaker et al.*, 2007a]. Measured average clast size in such catchments is ~0.1 m, while joint spacing in such catchments is a maximum of 0.3 m [*Whittaker et al.*, 2007b, 2010]. If a jointed block with the latter dimension provides the critical threshold needed to incise (a maximum end-member), a basal shear stress of ~145–290 Pa and discharge of 10–20 $m^3$/s is required for entrainment, using the channel geometries for F3 and F4 and assuming an appropriate value for the critical Shields Stress [*Whipple*, 2001; *Snyder et al.*, 2003; *Cowie et al.*, 2008].

These entrainment values are a small percentage of the bankfull total for these catchments. Consequently, while a critical threshold for erosion may well exist for the catchments in this study, we are not persuaded that a threshold can explain the trend in Figure 7. In fact, we have no evidence to support an inverse relationship between threshold and fault throw rate in general. Indeed, as bed load grain-size increases markedly for catchments crossing faster slipping faults [*Whittaker et al.*, 2010], this would generally act to increase the threshold and response time for such channels [cf. *Attal et al.*, 2011].

### 5.3. A Link Between Channel Slope, Hydraulic Geometry and Knickpoint Celerity?

[31] In the simple approximation for knickzone celerity in equation (2), channel gradient drops out of the equation for a unit stream power model with $n = 1$ leaving $m = 0.5$, if $W$ scales with $\sqrt{A}$, as is often assumed [*Whittaker et al.*, 2007b]. However, the relationship between faster knickpoint retreat rates and large fault throw rates is explainable if $\Psi_A$ implicitly embeds a nonlinear channel gradient effect (i.e., $\Psi_A = \Psi_K S^{n-1}$). For $n > 1$ a knickpoint will then migrate more rapidly on steeper channel slopes; such an outcome has been
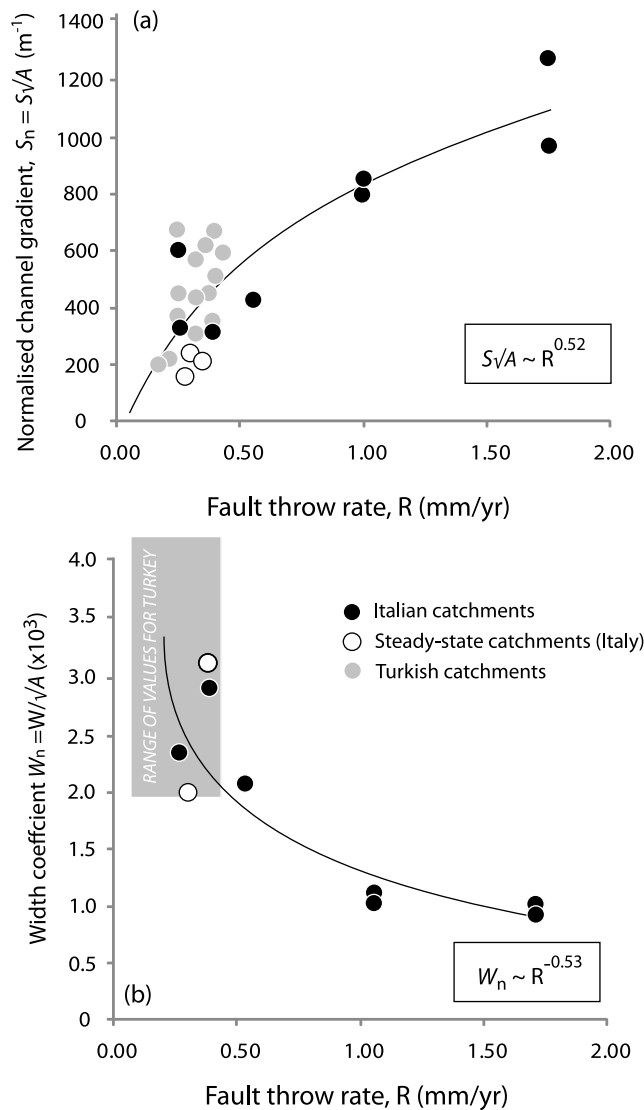
**Figure 8.** (a) Drainage area normalized channel slope, $S_n = S\sqrt{A}$ against fault throw rate, $R$. White circles represent channel gradients at the fault for catchments that have reached topographic steady state. Where the transient wave of incision had migrated more than 2 km upstream of the fault, we used the local knickzone gradient within 2 km of the knickpoints indicated by stars in Figure 4. Line shows best fit power law dependence of $S_n$ on $R$. (b) Mean knickzone channel width, $W_n$, normalized for drainage area at the fault, against fault throw rate, $R$, for Italy (points) and Turkey (box shows data range). Line shows best fit power law dependence of $W_n$ on $R$.

argued to fit the pattern of knickzone evolution in Eastern Australia [*Weissel and Seidl*, 1998]. This explanation requires channels that have undergone a greater tectonic perturbation (i.e., those crossing higher throw rate faults) to have steeper channel gradients in the knickzone upstream of the fault than slower moving faults. One way this could happen is if the higher relative throw rate, $R$, at the fault leads to the accumulation of more slip per unit time and hence a steeper long profile convexity [*Whittaker et al.*, 2008]. Figure 7b shows that $\Psi_A \sim R^{0.67}$. Making the ad hoc

assumption of a simple linear relationship between throw rates and channel gradient upstream of the fault, a stream power erosion law approximating these dynamics would therefore be of the form $E \sim A^{0.5} S^{1.67}$ (cf. equation (2)). The implied slope exponent $n = 1.67$, in this case is considerably higher than typical values of $0.7 < n < 1.3$ derived or assumed in many publications [e.g., *Tucker and Whipple*, 2002; *Wobus et al.*, 2006a; *Attal et al.*, 2008] and implies low steady state concavities.

[32] In fact, the relationship between current fault throw rate and average channel gradient in the knickzones of the Italian catchments is weak with channel slopes near the fault varying from <0.05 to >0.15 (Table 1); in part this reflects the fact that expected channel slope decreases with increasing catchment size. If we normalize these local slopes ($S_n$) for catchment size differences (Figure 8a) by multiplying the channel gradients by $\sqrt{A}$, analogous to calculating a steepness index [cf. *Wobus et al.*, 2006b], we find that $S_n \sim R^{0.52}$ (Figure 8a). In other words, channels in knickzones upstream of faults are steeper for the same drainage area when the fault throw rate is higher. But this relationship definitely cannot explain the signal in Figure 7 fully because the dependence of $S_n$ on fault throw rate is much less than the linear one we assumed above. The sublinear relationship would require the knickpoint retreat rate parameter, $\Psi_A \sim S^{1.28}$ to account for the trend in Figure 7 if all the knickpoint migration signal is to be explained by channel steepening alone. This dependency therefore implies $n \geq 2.28$ for a detachment limited stream power erosion law (equations (1) and (2)), which is physically improbable.

[33] However, channels can narrow significantly in regions of high uplift or steepness, particularly if they are undergoing a transient response to tectonics [*Finnegan et al.*, 2005; *Turowski et al.*, 2006; *Amos and Burbank*, 2007; *Whittaker et al.*, 2007a]. Shear stress per unit width on the bed increases, and thus erosivity and knickpoint retreat rates will increase [*Attal et al.*, 2008, 2011]. We evaluate whether the width narrowing, in addition to channel gradient steepening, is sufficient to explain our results by plotting drainage-area-normalized average channel widths (i.e., $W_n = W/\sqrt{A}$) for our study channels against fault throw rate, $R$ (Figure 8b). Channel widths are the average of all measurements taken in the knickzone upstream of the active fault, or within 2 km of the knickpoint (Figures 2 and 4) if the knickzone is longer than this, to keep the local variation in $A$ small (Table 1). We find that $W_n \sim R^{-0.53}$ so channels are indeed narrower for the same drainage area when the throw rate is greater. This trend in normalized channel width is similar to the finding by *Turowski et al.* [2006] from experimental results that the channel width prefactor decreases with uplift rate [see *Turowski et al.*, 2006, Figure 7], and is complementary to field and modeling studies which show that channels are narrower for the same drainage area when $S$ or $R$ is greater [e.g., *Finnegan et al.*, 2005; *Whittaker et al.*, 2007a; *Attal et al.*, 2008].

[34] An inspection of equation (1) shows that if $W \sim R^{-0.53}\sqrt{A}$, erosion rates should scale as $E \sim R^{0.53}A^{0.5}S^n$ for a typical unit stream power erosion law. Consequently, the drainage-area normalized knickzone parameter, $\Psi_A$, must also scale with $R^{0.53}$ by channel width narrowing alone (equation (2)), because our original $\Psi_A$ formulation for a unit stream power law clearly has an implicit but substantial

channel narrowing effect that we had not accounted for. Importantly, $\Psi_A \sim R^{0.53}$ accounts for most of the dependency of knickpoint retreat rate on fault throw rate deduced in Figure 7 (where $\Psi_A \sim R^{0.67}$). The link between knickpoint retreat rate and fault throw rate can therefore be explained largely by channel narrowing, leaving a small residual, not accounted for by width changes, of $\Psi_A \sim R^{0.14}$.

[35] The relationship between channel gradient and throw rate (Figure 8a) could account for this residual, but *only* as long as the slope exponent, $n$ (equations (1) and (2)) in the knickpoint celerity equation is larger than 1, so knickpoint retreat is positively correlated to slope. We do not know $n$ explicitly, but if the exponent $n$ were greater than one, combining the residual relationship of knickpoint retreat rate with fault throw rate ($\Psi_A \sim R^{0.14}$); the dependence of normalized channel gradient with fault throw ($S_n \sim R^{0.52}$; Figure 8a); and noting that $\Psi_A \sim S^{n-1}$; we calculate that $n > 1.3$ would be required to fully account for the residual knickpoint retreat rate trend. The required $n$ value is higher than many studies assume but it is consistent with estimates of some previous studies [e.g., *Attal et al.*, 2008].

### 5.4. A Role for Sediment in Modulating Fluvial Erosion Rates?

[36] While width narrowing plays an important role in setting knickpoint retreat rates in the case of bedrock rivers presented here, sediment input to such undersupplied rivers can enhance fluvial erosion rates over clear water conditions by acting as tools to scour the bed, while also limiting the rates of erosion due to coverage effects if sediment becomes abundant. However, the shape of this "erosional efficiency" function, $f(Q_s)$, is not fully constrained (equation (1)) [*Sklar and Dietrich*, 2004; *Gasparini et al.*, 2006; *Turowski et al.*, 2006; *Jansen et al.*, 2011]. *Cowie et al.* [2008] demonstrated clearly that differences in sediment supply can have a significant effect on landscape evolution over periods of $10^5$–$10^6$ years by comparing catchments in Italy and Greece crossing faults with similar tectonic histories, but differing sediment-mediated landscape responses. This work suggested that while the Italian catchments were very close to the detachment limited end-member, in detail they could be characterized by a small but incision-enhancing sediment supply that was 8–15% of the long-term transport capacity. *Jansen et al.* [2011] have also recently argued that elevated sediment supply boosted tool-driven knickpoint retreat in Scotland in the early Holocene, with retreat rates decreasing by up to an order of magnitude to the present day.

[37] Instead of explaining the residual relationship (i.e., that not explained by width narrowing) between knickpoint retreat rate and fault throw rate in rivers in Italy and Turkey by postulating that $n > 1$ in the standard stream power erosion law equation, an alternative hypothesis is that $n = 1$, but that the catchments do not quite lie at the detachment limited end-member, and therefore $f(Q_s) \neq 1$ (equation (1)). In this case enhanced sediment supply would help to drive faster knickpoint retreat on catchments crossing faults with high throw rates. For this to happen, we would require the sediment-mediated erosional efficiency increases as fault throw rate increases, so that the study rivers line up on the "tools-effect" rising-limb of the erosional efficiency curve with greater relative sediment supply [*Sklar and Dietrich*, 2004; *Cowie et al.*, 2008]. *Whittaker et al.* [2010] showed that

landsliding provides enhanced coarse sediment supply to catchments undergoing a transient response to faulting, and that this effect is increased when the tectonic perturbation is larger, so this explanation is plausible. However, our data do not allow us to separate, unambiguously, this effect on knickpoint retreat rate from the hypothesis that $n \geq 1.3$ (section 5.3) because we cannot accurately reconstruct the ratio of long-term sediment supply rates to sediment transport capacity in all our study catchments over million year timescales.

### 5.5. Climate Differences Between the Catchments

[38] The drainage-area-normalized knickzone migration rate parameter, $\Psi_A$, is at least twice as large in Italy, for rivers crossing faults with similar slip rates and drainage areas, suggesting that the rate of fault motion is not the only significant control on knickpoint migration. One explanation for the observed difference is that the relationship between drainage area and discharge in the two field areas is not the same. In simple terms, catchment discharge, $Q$, can be expressed as:

$$Q = pA^c, \tag{6}$$

where $p$ is a catchment averaged value that relates to the magnitude of precipitation and ground infiltration rates. $c$ is a positive exponent, often (and conveniently) taken to be 1, in which case drainage area is linearly proportional to discharge [e.g., *Cowie et al.*, 2008]. If the celerity of the transient incision wave (equation (3)) for a unit stream power model is explicitly expressed in terms of discharge rather than $A$, then we have:

$$C_E = k\sqrt{(pA_{f(L)})}, \tag{7}$$

where $k$ is a constant. Inspection of equation (7) and equation (3) immediately demonstrates that $\Psi_A = k\sqrt{p}$, for a fixed catchment drainage area. Consequently, a more than twofold increase in $\Psi_A$ could be directly explainable by an average more than fourfold increase in $p$, assuming there is no significant geomorphic discharge threshold that must be exceeded before fluvial incision can occur.

[39] Are the Turkish catchments drier, with greater infiltration than our Italian examples? To answer this question we can compare modern day climate records, but since 90% of the catchments' evolution took place outside of warm interglacial periods, we need to consider precipitation and ground condition estimates for glacial periods, such as the LGM (note that none of the channels contained valley glaciers in the last 1 My). Present-day annual precipitation for the city of L'Aquila, central Apennines, is ~750 mm/yr, while yearly rainfall estimates on the high Apennine mountains are 1200–1500 mm/yr in the Gran Sasso and Monte Maiella, respectively [*Massoli-Novelli and Pettita*, 1997; *Coltorti and Pieruccini*, 2006]. Average yearly rainfall in Antakya, southern Turkey, is ~1000 mm/yr but varies in the Hatay region from 500 mm/yr to 1500 mm/yr [*Casana*, 2008]. These data show that there is not much difference in the total rainfall received by the two areas at present.

[40] However, the detailed palaeoclimate and sedimentological data available for Italy and the Hatay (summarized in

sections 2.1 and 2.2) indicate that the Apennines were wetter during Pleistocene glacial periods so the studied catchments would have had elevated run-off by a factor of 2–4. By contrast, paleoclimate data suggest much of the Hatay area and the Levant coast were dryer by approximately a factor of 2, with some extremely arid phases where rainfall was up to ten times less than today [i.e., *Robinson et al.*, 2006]. So although the two study areas experience similar interglacial climates, glacial climatic conditions are highly dissimilar. Therefore, it is proposed that the climate differences resulted in the inferred factor of 4 difference in the ratio of precipitation to infiltration, *p*, required to resolve the twofold difference in drainage area normalized knickpoint migration rates between catchments eroding similar rock types and crossing faults with similar slip rates and in Turkey and Italy.

## 6. Implications and Conclusions

[41] Our results are important because knickpoint retreat rates fundamentally determine the timescale over which changes to tectono-climatic boundary conditions are transmitted to the landscape. First, our data demonstrates that a fluvial response time of 1–3 My is broadly appropriate for the characterization of a catchment response to a tectonic perturbation in two Mediterranean settings [cf. *Whittaker et al.*, 2007a; *Boulton and Whittaker*, 2009]. However, in detail for these rivers, which lie close to the detachment limited end-member, landscape response times are strongly linked to the magnitude of the tectonic perturbation and Quaternary climate. Our analysis indicates that an order of magnitude difference in fault throw rate can lead to a six- to sevenfold difference in knickpoint celerity, for otherwise similar catchments with identical drainage areas. This finding is important because it suggests that, counterintuitively, landscapes displaced from topographic steady state by a significant tectonic perturbation will actually re-attain steady state more rapidly than areas where the perturbation is smaller. We document that drainage-area-normalized knickpoint retreat rates scales as $\sim R^{0.67}$, which means that fault uplift rate is at least as important as catchment size in governing knickzone retreat rates. Geomorphic studies that ignore this effect could significantly overestimate landscape response times in tectonically active areas.

[42] While rock mass strength is often argued to play a significant role in modulating bedrock river incision rates [e.g., *Stock and Montgomery*, 1999], here we find that it does not make a noticeable difference to knickpoint retreat rates for catchments where average Selby values range from 55 to 75 RMS units. Instead we find that the dependence of knickpoint retreat rates on fault throw rates is largely explainable as a result of channel width changes. Consistent with theoretical, empirical and modeling studies [*Finnegan et al.*, 2005; *Turowski et al.*, 2006; *Whittaker et al.*, 2007b; *Attal et al.*, 2008, 2011], we find that both the Italian and Turkish channels have steeper narrower channel widths upstream for the same drainage area when they cross faster slipping fault blocks and this enhances knickpoint celerity for rivers crossing faults with high throw rates. In addition to this, we also find that drainage-area-normalized channel slopes are steeper upstream of high throw rate faults. This latter effect, in combination with the strong channel narrowing

signal, is sufficient to account for all the dependence of knickpoint retreat rate on fault uplift rate if $n \geq 1.3$ in the stream power erosion law, without needing to include threshold or sediment supply effects. However, we cannot rule out that $n = 1$, and that a small but incision-enhancing sediment "tools" effect boosted knickpoint retreat rates in addition to the documented width effects. Our results demonstrate that dynamic channel adjustment needs to be incorporated routinely into both field characterization of geomorphic systems perturbed by tectonics, and in landscape evolution models in order for them to produce robust model output [cf. *Attal et al.*, 2008].

[43] Finally, we show that knickpoints in Turkish catchments move at about half the rate of the Italian examples even when throw rates are similar and catchment size differences are taken into account and we suggest that this disparity is likely to be a climatic effect. While the magnitude of present-day precipitation does not vary significantly between the two areas, climate proxy data, modeling and sedimentological observations suggest that the Apennines were characterized by periglacial conditions that promoted enhanced runoff during much of the last 1 My, while southern Turkey was characterized by arid conditions where mean annual rainfall was typically half as much as the present interglacial, with occasional episodes of hyper-aridity. These data therefore suggest that climate variability also plays a role in modulating landscape response time over time periods of $10^6$ years.

[44] More widely this study demonstrates the importance of detailed studies of transient landscapes where the tectonic and climatic boundary conditions governing fluvial response times are well constrained independently. A key challenge for the future is to evaluate, for other tectonically active areas, the rate at which highly perturbed fluvial systems re-attain topographic steady state; such data are vital to constrain fully the time period over which transient landscapes act as a tectonic archive.

## Appendix A

[45] Indirect tests of rock hardness such as a Schmidt hammer or point load test are quick and cheap methods of determining the strength of a sample. However, point load testing does not give the uniaxial compressive strength (UCS) of a rock but rather a normalized rock strength index calculated from the dimensions of the sample and the load at which the rock failed [*Franklin*, 1985]. These indices can then be converted using well researched factors into UCS values for comparison with other methods, and for use within the rock mass strength assessment schemes, such as that proposed by *Selby* [1980]. *Sabatakakis et al.* [2008] determined the conversion factors for a range of sedimentary lithologies to convert point load results ($I_{s(50)}$) to UCS values. Using a linear regression three different point load strength classes were identified from a range of lithologies, each with a different relationship to the UCS (equations (A1)–(A3)), with class I roughly being equivalent to marl and classes II and III being limestone and sandstone of different strength.

$$UCS(\sigma_c) = 13I_{s(50)} \quad \text{for rocks with a point load strength}$$
$$< 2 \text{ MPa, class I} \tag{A1}$$

$$UCS(\sigma_c) = 24I_{s(50)} \text{ for rocks with a point load strength}$$
$$2\text{–}5 \text{ MPa, class II} \tag{A2}$$

$$UCS(\sigma_c) = 28I_{s(50)} \text{ for rocks with a point load strength}$$
$$>5 \text{ MPa, class III} \tag{A3}$$

*Diamantis et al.* [2009] conducted similar experiments on serpentinites, determining the conversion factor from ($I_{s(50)}$) to UCS again to be a linear relationship (equation (A4)):

$$UCS(\sigma_c) = 19.79I_{s(50)}. \tag{A4}$$

By contrast, a Schimdt hammer measures the in situ rebound of a spring loaded mass against a hard surface. Typically a number of readings (e.g., 20) are taken for each lithology or site and the average reading is then used. These readings can be directly incorporated into a rock mass strength assessment scheme such as *Selby* [1980]. Additionally, the rebound number can also be converted to UCS by reference to the conversion chart supplied on the side of each Schmidt hammer.

[46] The well-known rock mass strength scheme (RMS) of *Selby* [1980] was used in the field to assess the variation in lithological competence across the catchments. Typical rocks have Selby values of ~40 ("weak") to greater than 70 ("strong") [e.g., *Whittaker et al.*, 2008]. The scheme breaks down rock strength into 7 constituent areas, which are assigned a value and weighted for their proportional contribution to rock strength *in toto* [*Selby*, 1980, Table 6.2] on the basis of Selby's original field observations. The categories comprise:

[47] (i) Intact rock strength from UCS or Schmidt hammer readings (up to 20 percentage points of the Selby RMS), ranging from rocks with a UCS of 1–25 MPa or Schmidt hammer R values of <35 scoring as little as 5 percentage points, and rocks with a UCS of >200 MPa/Schmidt hammer R values >60 scoring the full 20 percentage points available (Table 1) [*Selby*, 1980].

[48] (ii) Degree of weathering (up to 10 percentage points of Selby RMS, using a 5 point qualitative scale from "unweathered" to "completely weathered").

[49] (iii) Joint spacing (up to 30 percentage points of the Selby RMS, from >3 m spacing to <50 mm spacing).

[50] (iv) Joint orientation (up to 20 percentage points of the Selby RMS, depending on whether the joints dip in or out of the slope, and at what angle).

[51] (v) Joint width (up to 7 percentage points of the Selby RMS, depending on whether the joints are >20 mm thick, or as low 0.1 mm thick).

[52] (vi) Joint continuity (7% of the Selby value on a qualitative scale that covers the degree of connectedness and the degree of infill).

[53] (vii) The presence and discharge of groundwater outflow (6% of the value, on a five point scale that ranges from none to a discharge of >125 L/min/10 m$^2$).

[54] The total Selby RMS quoted is the sum of each of the % point values ascribed in each subclass given above, with error bars relating to the range of values ascribed in the field.

## References

Allen, J. R. M., W. A. Watts, and B. Huntley (2000), Weichselian palynostratigraphy, palaeovegetation and palaeoenvironment: The record from the Lago Grande di Monticchio, southern Italy, *Quat. Int.*, *73–74*, 91–110, doi:10.1016/S1040-6182(00)00067-7.

Allen, P. A. (2008), From landscapes into geological history, *Nature*, *451*, 274–276, doi:10.1038/nature06586.

Amos, C. B., and D. W. Burbank (2007), Channel width response to differential uplift, *J. Geophys. Res.*, *112*, F02010, doi:10.1029/2006JF000672.

Attal, M., G. E. Tucker, A. C. Whittaker, P. A. Cowie, and G. P. Roberts (2008), Modeling fluvial incision and transient landscape evolution: Influence of dynamic channel adjustment, *J. Geophys. Res.*, *113*, F03013, doi:10.1029/2007JF000893.

Attal, M., P. A. Cowie, A. C. Whittaker, D. Hobley, G. E. Tucker, and G. P. Roberts (2011), Testing fluvial erosion models using the transient response of bedrock rivers to tectonic forcing in the Apennines, Italy, *J. Geophys. Res.*, *116*, F02005, doi:10.1029/2010JF001875.

Bar-Matthews, M., A. Ayalon, and A. Kaufman (1997), Late Quaternary paleoclimate in the eastern Mediterranean region from stable isotope analysis of speleothems at Soreq Cave, Israel, *Quat. Res.*, *47*, 155–168, doi:10.1006/qres.1997.1883.

Bar-Matthews, M., A. Ayalon, M. Gilmour, A. Matthews, and C. J. Hawkesworth (2003), Sea-land oxygen isotopic relationships from planktonic foraminifera and speleotherms in the Eastern Mediterranean region and their implication for paleorainfall during interglacial intervals, *Geochim. Cosmochim. Acta*, *67*, 3181–3199, doi:10.1016/S0016-7037(02)01031-1.

Berlin, M. M., and R. S. Anderson (2007), Modeling knickpoint retreat on the Roan Plateau, western Colorado, *J. Geophys. Res.*, *112*, F03S06, doi:10.1029/2006JF000553.

Berlin, M. M., and R. S. Anderson (2009), Steepened channels upstream of knickpoints: Controls on relict landscape response, *J. Geophys. Res.*, *114*, F03018, doi:10.1029/2008JF001148.

Bishop, P., T. B. Hoey, J. D. Jansen, and I. L. Artza (2005), Knickpoint recession rate and catchment area: The case of uplifted rivers in Eastern Scotland, *Earth Surf. Processes Landforms*, *30*, 767–778, doi:10.1002/esp.1191.

Bogaart, P., G. Tucker, and J. De Vries (2003), Channel network morphology and sediment dynamics under alternating periglacial and temperate regimes: A numerical simulation study, *Geomorphology*, *54*, 257–277, doi:10.1016/S0169-555X(02)00360-4.

Boulton, S. J., and A. H. F. Robertson (2007), The Miocene of the Hatay area, S Turkey: Transition from the Arabian passive margin to an underfilled foreland basin related to closure of the southern Neotethys Ocean, *Sediment. Geol.*, *198*, 93–124, doi:10.1016/j.sedgeo.2006.12.001.

Boulton, S. J., and A. H. F. Robertson (2008), The Neogene-Recent Hatay Graben, south-central Turkey: Graben formation in a setting of oblique extension (transtension) related to post-collisional tectonic escape, *Geol. Mag.*, *145*, 800–821, doi:10.1017/S0016756808005013.

Boulton, S. J., and A. C. Whittaker (2009), Quantifying the slip-rates, spatial distribution and evolution of active normal faults from geomorphic analysis: Field examples from an oblique-extensional graben, southern Turkey, *Geomorphology*, *104*, 299–316, doi:10.1016/j.geomorph.2008.09.007.

Boulton, S. J., A. H. F. Robertson, and U. C. Ünlügenç (2006), Tectonic and sedimentary evolution of the Cenozoic Hatay Graben, southern Turkey: A two-phase, foreland basin then transtensional basin model, *Geol. Soc. Spec. Publ.*, *260*, 613–634, doi:10.1144/GSL.SP.2006.260.01.26.

Boulton, S. J., A. H. F. Robertson, R. M. Ellam, Ü. Şafak, and U. C. Ünlügenç (2007), Strontium isotopic and micropalaeontological dating used to help redefine the stratigraphy of the neotectonic Hatay Graben, southern Turkey, *Turk. J. Earth Sci.*, *16*, 141–178.

Brocklehurst, S. H. (2010), Tectonics and geomorphology, *Prog. Phys. Geogr.*, *34*, 357–383, doi:10.1177/0309133309360632.

Casana, J. (2008), Mediterranean valleys revisited: Linking soil erosion, land use and climate variability in the northern Levant, *Geomorphology*, *101*, 429–442, doi:10.1016/j.geomorph.2007.04.031.

Cavinato, G. P., and P. G. DeCelles (1999), Extensional basins in tectonically bi-modal central Apennines fold-thrust belt, Italy: Response to corner flow above a subducting slab in retrograde motion, *Geology*,

27, 955–958, doi:10.1130/0091-7613(1999)027<0955:EBITTB>2.3.CO;2.

Cavinato, G. P., C. Carusi, M. Dall'Asta, E. Miccadei, and T. Piacentini (2002), Sedimentary and tectonic evolution of Plio–Pleistocene alluvial and lacustrine deposits of Fucino Basin (central Italy), *Sediment. Geol.*, *148*, 29–59.

Coltorti, M., and P. Pierucini (2006), The last interglacial pedocomplexes in the litho- and morpho-stratigraphical framework of the central-northern Apennines (central Italy), *Quat. Int.*, *156–157*, 118–132, doi:10.1016/j.quaint.2006.05.025.

Cowie, P. A., and G. P. Roberts (2001), Constraining slip rates and spacings for active normal faults, *J. Struct. Geol.*, *23*, 1901–1915, doi:10.1016/S0191-8141(01)00036-0.

Cowie, P. A., A. C. Whittaker, M. Attal, G. E. Tucker, G. P. Roberts, and A. Ganas (2008), New constraints on sediment-flux dependent river incision: Implications for extracting tectonic signals from river profiles, *Geology*, *36*, 535–538, doi:10.1130/G24681A.1.

Crosby, B. T., and K. X. Whipple (2006), Knickpoint initiation and distribution within fluvial networks, 236 waterfalls in the Waipaoa River, North Island, New Zealand, *Geomorphology*, *82*, 16–38, doi:10.1016/j.geomorph.2005.08.023.

D'Agostino, N., J. A. Jackson, F. Dramis, and R. Funiciello (2001), Interactions between mantle upwelling, drainage evolution and active normal faulting: An example from the central Apennines (Italy), *Geophys. J. Int.*, *147*, 475–497, doi:10.1046/j.1365-246X.2001.00539.x.

Diamantis, K., E. Gartzosa, and G. Migirosa (2009), Study on uniaxial compressive strength, point load strength index, dynamic and physical properties of serpentinites from central Greece: Test results and empirical relations, *Eng. Geol. Amsterdam*, *108*, 199–207, doi:10.1016/j.enggeo.2009.07.002.

DiBiase, R. A., K. X. Whipple, A. M. Heimsath, and W. B. Ouimet (2010), Landscape form and millennial erosion rates in the San Gabriel Mountains, CA, *Earth Planet. Sci. Lett.*, *289*, 134–144, doi:10.1016/j.epsl.2009.10.036.

Dorsey, R. J., and J. J. Roering (2006), Quaternary landscape evolution in the San Jacinto fault zone, Peninsular Ranges of southern California: Transient response to strike-slip fault initiation, *Geomorphology*, *73*, 16–32, doi:10.1016/j.geomorph.2005.06.013.

Erdik, M., N. Aydınoğlu, A. Pınar, and D. Kalafat (1997), *Report of Hatay Earthquake*, Kandilli Obs., Istanbul, Turkey.

Finnegan, N. J., G. Roe, D. R. Montgomery, and B. Hallet (2005), Controls on the channel width of rivers: Implications for modeling fluvial incision of bedrock, *Geology*, *33*, 229–232, doi:10.1130/G21171.1.

Franklin, J. A. (1985), Suggested method for determining point-load strength, *Int. J. Mech. Min. Sci. Geomech. Abstr.*, *22*, 51–60, doi:10.1016/0148-9062(85)92327-7.

Gasparini, N. M., R. L. Bras, and K. X. Whipple (2006), Numerical modeling of non–steady-state river profile evolution using a sediment-flux-dependent incision model, *Geol. Soc. Am. Spec. Pap.*, *398*, 127–141, doi:10.1130/2006.2398(08).

Giraudi, C. (1989), Lake levels and climate for the last 30,000 years in the Fucino area (Abruzzo–central Italy)–A review, *Palaeogeogr. Palaeoclimatol. Palaeoecol.*, *70*, 249–260, doi:10.1016/0031-0182(89)90094-1.

Giraudi, C., and M. Frezzotti (1997), Late Pleistocene glacial events in the central Apennines, Italy, *Quat. Res.*, *48*, 280–290, doi:10.1006/qres.1997.1928.

Harkins, N., E. Kirby, A. Heimsath, R. Robinson, and U. Resier (2007), Transient fluvial incision in the headwaters of the Yellow River, northeastern Tibet, China, *J. Geophys. Res.*, *112*, F03S04, doi:10.1029/2006JF000570.

Howard, A. D., W. E. Dietrich, and M. A. Seidl (1994), Modeling fluvial erosion on regional to continental scales, *J. Geophys. Res.*, *99*(B7), 13,971–13,986, doi:10.1029/94JB00744.

Jansen, J. D., D. Fabel, P. Bishop, S. Xu, C. Schnabel, and A. T. Codilean (2011), Does decreasing paraglacial sediment supply slow knickpoint retreat?, *Geology*, *39*, 543–546, doi:10.1130/G32018.1.

Jost, A., D. Lunt, M. Kageyama, A. Abe-Ouchi, O. Peyron, P. J. Valdes, and G. Ramstein (2005), High-resolution simulations of the last glacial maximum climate over Europe: A solution to discrepancies with continental palaeoclimatic reconstructions?, *Clim. Dyn.*, *24*, 577–590, doi:10.1007/s00382-005-0009-4.

Kettner, A. J., and J. P. M. Syvitski (2008), Predicting discharge and sediment flux of the Po River, Italy since the Last Glacial Maximum, in *Analogue and Numerical Forward Modelling of Sedimentary Systems: From Understanding to Prediction*, *Int. Assoc. of Sedimentol. Spec. Publ.*, vol. 40, edited by P. L. de Boer et al., pp. 171–190, Wiley-Blackwell, Chichester, U. K.

Kirby, E., K. X. Whipple, W. Tang, and Z. Chen (2003), Distribution of active rock uplift along the eastern margin of the Tibetan Plateau: Inferences from bedrock channel longitudinal profiles, *J. Geophys. Res.*, *108*(B4), 2217, doi:10.1029/2001JB000861.

Lavecchia, G., F. Brozzetti, M. Barchi, M. Menichetti, and J. V. A. Keller (1994), Seismotectonic zoning in east-central Italy deduced from an analysis of the Neogene to present deformations and related stress fields, *Geol. Soc. Am. Bull.*, *106*, 1107–1120, doi:10.1130/0016-7606(1994)106<1107:SZIECI>2.3.CO;2.

Massoli-Novelli, R., and M. Pettita (1997), Hydrogeological impact of the Gran Sasso Tunnels (Abruzzi, Italy), in *Engineering Geology and the Environment*, vol. 3, edited by P. G. Marinos et al., pp. 2787–2792, Balkema, Rotterdam, Netherlands.

Meadows, J. (2005), The Younger Dryas episode and the radiocarbon chronologies of the Lake Huleh and Ghab Valley pollen diagrams, Israel and Syria, *Holocene*, *15*, 631–636, doi:10.1191/0959683605hl838fa.

Mudd, S. M., and D. J. Furbish (2007), Responses of soil-mantled hillslopes to transient channel incision rates, *J. Geophys. Res.*, *112*, F03S18, doi:10.1029/2006JF000516.

Över, S., U. C. Ünlügenç, and O. Bellier (2002), Quaternary stress regime change in the Hatay region SE Turkey, *Geophys. J. Int.*, *148*, 649–662, doi:10.1046/j.1365-246X.2002.01621.x.

Palumbo, L., L. Bourles, A. Cinque, and R. Finkel (2004), Slip history of the Magnola fault (Apennines, central Italy) from $^{36}CI$ surface exposure dating: Evidence for strong earthquakes over the Holocene, *Earth Planet. Sci. Lett.*, *225*, 163–176, doi:10.1016/j.epsl.2004.06.012.

Pantosti, D., G. D'Addezio, and F. R. Cinti (1996), Paleoseismicity of the Ovindoli–Pezza fault, central Apennines, Italy: A history including a large, previously unrecorded earthquake in the Middle Ages (860–1300 A.D.), *J. Geophys. Res.*, *101*(B3), 5937–5959, doi:10.1029/95JB03213.

Ramrath, A., B. Zolitschka, S. Wulf, and J. F. W. Negendank (1999), Late Pleistocene climatic variations as recorded in two Italian maar lakes (Lago di Mezzano, Lago Grande di Monticchio), *Quat. Sci. Rev.*, *18*, 977–992, doi:10.1016/S0277-3791(99)00009-8.

Reinhardt, L. J., P. Bishop, T. B. Hoey, T. J. Dempster, and D. C. W. Sanderson (2007), Quantification of the transient response to base level fall in a small mountain catchment: Sierra Nevada, southern Spain, *J. Geophys. Res.*, *112*, F03S05, doi:10.1029/2006JF000524.

Roberts, G. P., and A. M. Michetti (2004), Spatial and temporal variations in growth rates along active normal fault systems: An example from the Lazio-Abruzzo, central Italy, *J. Struct. Geol.*, *26*, 339–376, doi:10.1016/S0191-8141(03)00103-2.

Robinson, S. A., S. Black, B. W. Sellwood, and P. J. Valdes (2006), A review of palaeoclimates and palaeoenvironments in the Levant and eastern Mediterranean from 25,000 to 5000 years BP: Setting the environmental background for the evolution of human civilisation, *Quat. Sci. Rev.*, *25*, 1517–1541, doi:10.1016/j.quascirev.2006.02.006.

Rossignol-Strick, M. (1995), Sea-land correlation of pollen records in the eastern Mediterranean for the glacial-interglacial transition: Biostratigraphy versus radiometric time-scale, *Quat. Sci. Rev.*, *14*, 893–915, doi:10.1016/0277-3791(95)00070-4.

Sabatakakis, N., G. Koukis, G. Tsiambaos, and S. Papanakli (2008), Index properties and strength variation controlled by microstructure for sedimentary rocks, *Eng. Geol. Amsterdam*, *97*, 80–90, doi:10.1016/j.enggeo.2007.12.004.

Selby, M. J. (1980), A rock mass strength classification for geomorphic purposes: With tests from Antarctica and New Zealand, *Z. Geomorphol.*, *24*, 31–51.

Sklar, L. S., and W. E. Dietrich (2004), A mechanistic model for river incision into bedrock by saltating bed load, *Water Resour. Res.*, *40*, W06301, doi:10.1029/2003WR002496.

Snyder, N. P., K. X. Whipple, G. E. Tucker, and D. J. Merritts (2003), Importance of a stochastic distribution of floods and erosion thresholds in the bedrock river incision problem, *J. Geophys. Res.*, *108*(B2), 2117, doi:10.1029/2001JB001655.

Stock, J. D., and D. R. Montgomery (1999), Geologic constraints on bedrock river incision using the stream power law, *J. Geophys. Res.*, *104*(B3), 4983–4993, doi:10.1029/98JB02139.

Tucker, G. E. (2009), Natural experiments in landscape evolution, *Earth Surf. Processes Landforms*, *34*, 1450–1460, doi:10.1002/esp.1833.

Tucker, G. E., and K. X. Whipple (2002), Topographic outcomes predicted by stream erosion models: Sensitivity analysis and intermodel comparison, *J. Geophys. Res.*, *107*(B9), 2179, doi:10.1029/2001JB000162.

Tucker, G. E., S. Lancaster, N. Gasparini, and R. Bras (2001), The Channel-Hillslope Integrated Landscape Development model (*CHILD*), in *Landscape Erosion and Evolution Modeling*, edited by R. S. Harmon and W. W. Doe III, pp. 349–388, Kluwer Acad./Plenum, New York.

Tucker, G. E., S. W. McCoy, A. C. Whittaker, G. P. Roberts, S. T. Lancaster, and R. Phillips (2011), Geomorphic significance of post glacial bedrock scarps on normal fault footwalls, *J. Geophys. Res.*, *116*, F01022, doi:10.1029/2010JF001861.

Turowski, J. M., D. Lague, A. Crave, and N. Hovius (2006), Experimental channel response to tectonic uplift, *J. Geophys. Res.*, *111*, F03008, doi:10.1029/2005JF000306.

Wegmann, K. W., and F. J. Pazzaglia (2009), Late Quaternary fluvial terraces of the Romagna and Marche Apennines, Italy: Climatic, lithologic, and tectonic controls on terrace genesis in an active orogen, *Quat. Sci. Rev.*, *28*, 137–165, doi:10.1016/j.quascirev.2008.10.006.

Weissel, J. K., and M. A. Seidl (1998), Inland propagation of erosional escarpments and river profile evolution across the southeast Australian passive continental margin, in *Rivers Over Rock: Fluvial Processes in Bedrock Channels, Geophys. Monogr. Ser.*, vol. 107, edited by J. Tinkler and E. Wohl, pp. 189–206, AGU, Washington, D. C., doi:10.1029/GM107p0189.

Whipple, K. X. (2001), Fluvial landscape response time: How plausible is steady-state denundation?, *Am. J. Sci.*, *301*, 313–325, doi:10.2475/ajs.301.4-5.313.

Whipple, K. X., and G. E. Tucker (1999), Dynamics of the stream-power river incision model: Implications for height limits of mountain ranges, landscape response timescales, and research needs, *J. Geophys. Res.*, *104*(B8), 17,661–17,674, doi:10.1029/1999JB900120.

Whipple, K. X., and G. E. Tucker (2002), Implications of sediment-flux-dependent river incision models for landscape evolution, *J. Geophys. Res.*, *107*(B2), 2039, doi:10.1029/2000JB000044.

Whipple, K. X., G. S. Hancock, and R. S. Anderson (2000), River incision into bedrock: Mechanics and relative efficacy of plucking, abrasion and cavitation, *Geol. Soc. Am. Bull.*, *112*, 490–503, doi:10.1130/0016-7606 (2000)112<490:RIIBMA>2.0.CO;2.

Whittaker, A. C., P. A. Cowie, M. Attal, G. E. Tucker, and G. Roberts (2007a), Bedrock channel adjustment to tectonic forcing: Implications for predicting river incision rates, *Geology*, *35*, 103–106, doi:10.1130/G23106A.1.

Whittaker, A. C., P. A. Cowie, M. Attal, G. E. Tucker, and G. P. Roberts (2007b), Contrasting transient and steady-state rivers crossing active normal faults: New field observations from the central Apennines, Italy, *Basin Res.*, *19*, 529–556, doi:10.1111/j.1365-2117.2007.00337.x.

Whittaker, A. C., M. Attal, P. A. Cowie, G. E. Tucker, and G. Roberts (2008), Decoding temporal and spatial patterns of fault uplift using transient river long profiles, *Geomorphology*, *100*, 506–526, doi:10.1016/j.geomorph.2008.01.018.

Whittaker, A. C., M. Attal, and P. Allen (2010), Characterising the origin, nature and fate of sediment exported from catchments perturbed by active tectonics, *Basin Res.*, *22*, 809–828, doi:10.1111/j.1365-2117.2009.00447.x.

Wobus, C., K. X. Whipple, E. Kirby, N. Snyder, J. Johnson, K. Spyropolou, B. Crosby, and D. Sheehan (2006a), Tectonics from topography: Procedures, promise, and pitfalls, *Spec. Pap. Geol. Soc. Am.*, *398*, 55–74, doi:10.1130/2006.2398(04).

Wobus, C. W., B. T. Crosby, and K. X. Whipple (2006b), Hanging valleys in fluvial systems: Controls on occurrence and implications for landscape evolution, *J. Geophys. Res.*, *111*, F02017, doi:10.1029/2005JF000406.